Journal of South American Earth Sciences 37 (2012) 77–94

Contents lists available at SciVerse ScienceDirect

Journal of South American Earth Sciences

journal homepage: www.elsevier.com/locate/jsames

Detrital zircon U–Pb ages of metasedimentary rocks from Sierra de Valle Fértil: Entrapment of Middle and Late Cambrian marine successions in the deep roots of the Early Ordovician Famatinian arc

E.A. Cristofolini [a,b,*], J.E. Otamendi [a,b], M.N. Ducea [c], D.M. Pearson [c], A.M. Tibaldi [a,b], I. Baliani [a]

[a] Departamento de Geología, Universidad Nacional de Río Cuarto, X5804BYA Río Cuarto, Argentina
[b] Consejo Nacional de Investigaciones Científicas y Técnicas, Argentina
[c] Department of Geosciences, University of Arizona, Tucson, AZ 85721, USA

ARTICLE INFO

Article history:
Received 29 June 2011
Accepted 21 February 2012

Keywords:
Detrital zircons
Geochronology
Metasedimentary rocks
Famatinian arc
West Gondwana

ABSTRACT

We obtained detrital zircon ages from three metasedimentary rocks with siliciclastic protoliths that were buried to paleodepths of 20–27 km during Early Ordovician Famatinian arc magmatism. In all three samples, U–Pb zircon age distributions are polymodal but the dominant peaks make well-defined clusters, matching the ages of orogenic systems that characterize West Gondwana. The most prominent peaks of constituent age populations at 520 Ma, 600 Ma, and 1050 Ma reflect derivation from sources that are characteristic of the West Gondwana margin. Moreover, grains with Meso- and Paleo-Proterozoic ages appear as small fractions (<5%). The siliciclastic protoliths to metasedimentary rocks from the deep Famatinian crust are dominantly composed of detritus derived from two sources: 1) a nearby magmatic arc or a rapidly exhuming orogen, and 2) sedimentary recycling of Neoproterozoic–Lower Cambrian sedimentary successions broadly grouped as Puncoviscana Formation. Our findings reveal that granulite–facies metasedimentary rocks in the deep crust of the Famatinian arc have detrital zircon patterns closely resembling those found in nearby Middle to Upper Cambrian quartz-rich turbidite sequences from central Famatina, the Cordillera Oriental and the Puna. At the regional scale, these sedimentary successions yield maximum depositional ages corresponding to the Middle Cambrian (<520 Ma). This indicates that metasedimentary rocks in the Sierra de Valle Fértil were rapidly buried to deep levels after deposition. Our results are also consistent with the existence of a crustal scale paleo-suture located at the western margin of the Sierras Valle Fértil and La Huerta that explains the differences of detrital zircon age patterns between metasedimentary rocks in the Valle Fértil and age-equivalent sedimentary units in the nearby Cuyania Terrane.

1. Introduction

Several recently-published studies addressed the sedimentary provenances of basins peripheral to western Gondwana (e.g., Schwartz and Gromet, 2004; Rapela et al., 2007; Adams et al., 2008, 2010; Drobe et al., 2009; Collo et al., 2009; Verdecchia et al. 2011). Taken as a whole, these studies yielded two major results: 1- metasedimentary rocks deposited in Lower Paleozoic basins and derived from West Gondwana masses are fingerprinted by the existence of a prominent cluster of detrital zircon ages reflecting the Brasiliano/Pan-African orogenies; and 2- the widespread presence of zircon grains of about 1000 Ma do not permit a distinction between Gondwanan and Laurentian sources. This previous work set the basis for the present contribution.

U–Pb zircon geochronology by laser-ablation inductively-coupled-plasma mass spectrometry (e.g., Gehrels et al., 2008) was applied to three detrital samples to better constrain ages of deposition, magmatism and metamorphism within the Sierra de Valle Fértil section, which is thought to expose lower crustal levels of the Early Ordovician Famatinian arc. Correlation of our measured detrital zircon (DZ) spectra with those exhibited by strata of West Gondwana helps constrain the early Paleozoic geological evolution of the Sierra de Valle Fértil. Additionally, the subsequent deep-crustal burial of these metasediments to granulite–facies conditions during Early Ordovician Famatinian magmatism provides one of the few records for reconstructing the early geologic history of this arc system.

* Corresponding author. Tel.: +54 358 4676198; fax: +54 358 4680280.
E-mail address: ecristofolini@exa.unrc.edu.ar (E.A. Cristofolini).

0895-9811/$ – see front matter © 2012 Elsevier Ltd. All rights reserved.
doi:10.1016/j.jsames.2012.02.001

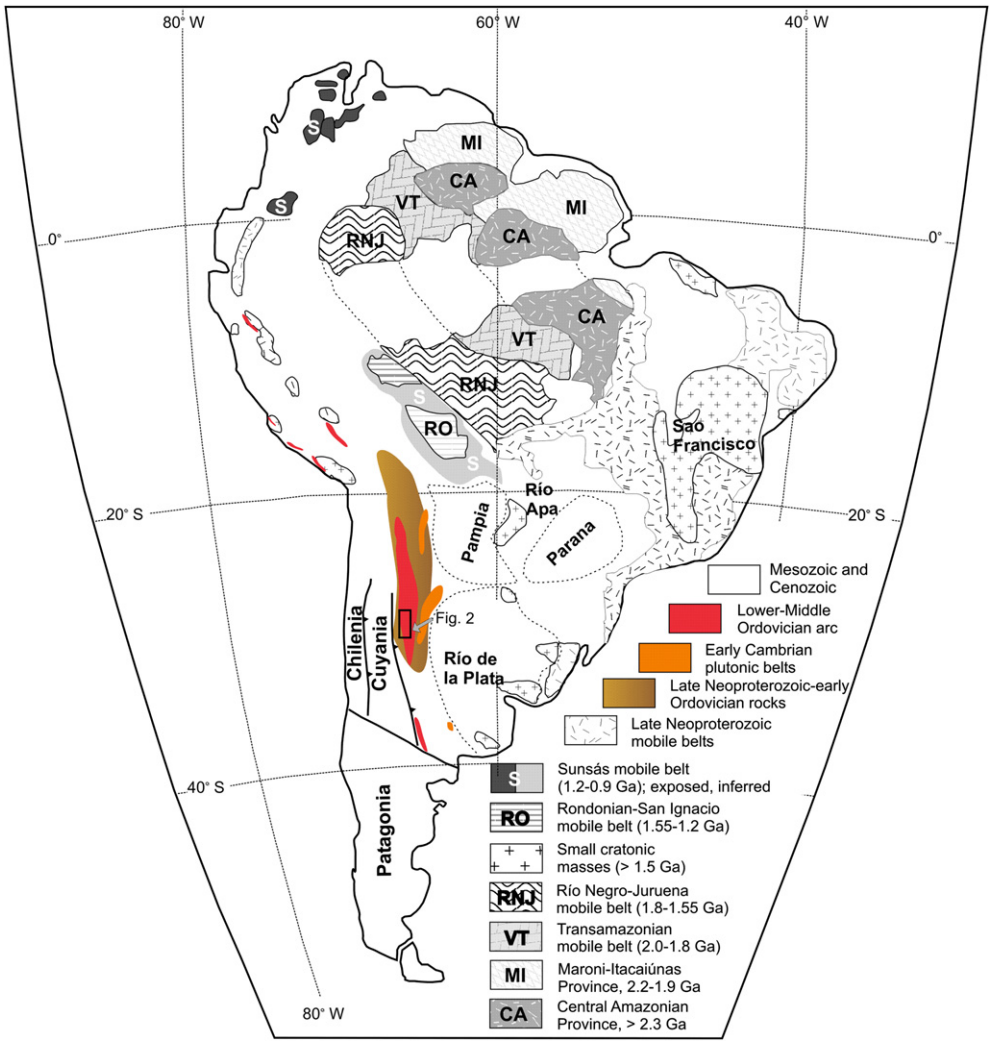

Fig. 1. Generalized geological map of South America presented by Cordani et al. (2000), here adapted from the modified version by Bahlburg et al. (2009). The map also incorporates some geological features taken after Chew et al. (2007), Rapela et al. (2007) and Chernicoff et al. (2010). The South American map outlines the geological framework for the Early Ordovician Famatinian-Puna arc. Excluding the Andean orogenic system, the geology of South America is dominated by the presence of Archaean to Mesoproterozoic cratonic landmasses that are bordered and joined by Proterozoic and Paleozoic orogenic and magmatic belts.

2. Geological settings for the Ordovician active margin of the West Gondwana

The subduction-related Ordovician arc extends for about 2000 km along the Andes from northern Peru to central Argentina (Fig. 1; e.g., Chew et al., 2007; Chernicoff et al., 2010). This magmatic belt has long been considered to have developed on several Precambrian landmasses that assembled to form West Gondwana (Pankhurst et al., 1998; Lucassen and Franz, 2005; Bahlburg et al., 2006; Ramos et al., 2010). Given that West Gondwana was assembled after closure of the Adamastor Ocean (between the Brazilian and southwest African cratonic masses) and the Mozambique Ocean (between East and West Gondwana landmasses) in Late Cambrian times (e.g., Vaughan and Pankhurst, 2008), the Early Ordovician magmatic arc is the earliest subduction-related plutonic–volcanic belt currently showing long segments of the West Gondwanan margin. This Early Ordovician arc was also part of one of the largest and longest-lived accretionary orogens in Earth history, extending along the margin of Gondwana from Australia through the Pacific border of Antarctica to the northern Andes (Cawood, 2005; Vaughan et al., 2005; Cawood and Buchan, 2007).

Table 1
Location, mineral composition, and condition of metamorphism of metasedimentary rocks selected for analyzing detrital zircon.

Sample	VFSCH22	VFNO28	VFNO49
Latitude South	30°52′13.7″	30°12′52.8″	30°16′49.5″
Longitude West	67°35′46.9″	67°49′3.5″	67°49′49.8″
Modal composition			
Quartz	50	34	42
Plagioclase (An)	24 (0.25)	32 (0.33)	24 (0.25)
K-feldspar			6
Biotite (Mg#)	20 (0.59)	16 (0.59–0.64)	16 (0.63)
Garnet (Mg#)	3 (0.32)	2	3 (0.36)
Cordierite (Mg#)		15 (0.76)	7 (0.77)
Sillimanite	2		
Oxides	1	1	< 1
Others	Zrn, Ap, Mzn, Ser	Zrn, Ap, Spl, Ser	Zrn, Ap, Ser
Inferred protolith	Lithic arenite	Shale	Graywacke
Temperature at metamorphic peak	850 ± 50 °C		830 ± 50 °C
Pressure at metamorphic peak	8.2 ± 0.5 kbar		7.1 ± 0.5 kbar

Modal proportion is determined by point counting (at least 2000 points). (An) denotes anorthite mole fraction of the plagioclase; while (Mg#) is for the $Mg/Mg + Fe^{2+}$ ratio based on cation proportions per formulae unit. Mineral compositions are from our unpublished dataset, whilst thermal and baric conditions attained at metamorphic peak are on average estimates with conventional geothermobarometric methods.

In the modern configuration, the basement geology east of the early Paleozoic continental paleo-margin is characterized by a series of Precambrian basement terranes and Neoproterozoic belts formed during Pan-African and Brasiliano orogenesis (Fig. 1; de Brito Neves and Cordani, 1991; Trompette, 1997). Several cratons made up West Gondwana, but few were close to Early Ordovician active margin (Fig. 1), among these are Río de la Plata, Luis Alvés, Rio Apa, Kalahari and Amazonia, which were dominated by Paleo- and Mesoproteroic crystalline rocks (de Brito Neves and Cordani, 1991; Rapela et al., 2007; Cordani et al., 2009). These old cratonic masses were surrounded by wide Neoproterozoic (Brasiliano–Pan-African) orogenic belts (Trompette, 1997; Cordani et al., 2009; Ramos et al., 2010).

As observed over large regions of northwestern Argentina, Pampean orogenesis resulted in uplift and exposure of thick uppermost Neoproterozoic and lower Cambrian turbidite sequences deposited on the margin of Gondwana (Ježek et al., 1985; Aceñolaza and Durand, 1986). These turbidite successions are broadly named Puncoviscana Formation; their metamorphic grade and depth of exhumation generally increase toward the south (Rapela et al., 1998; Schwartz and Gromet, 2004). Pressure–temperature (*P–T*) paths of the most deeply exhumed metamorphic rocks (granulite–facies equivalent conditions) demonstrate an intense tectono-thermal event that was followed by relatively rapid unroofing (Rapela et al., 1998; Otamendi et al., 2004). In the north (23°–25° south latitude), a plutonic belt intruded into the Puncoviscana Formation during late Early Cambrian time (ca. 520 Ma; Hongn et al., 2010). This plutonism seems to reflect the development of a late Pampean subduction-related system that did not evolve into a large and long-lived magmatic arc (Rapela et al., 1998). However, a short-lived

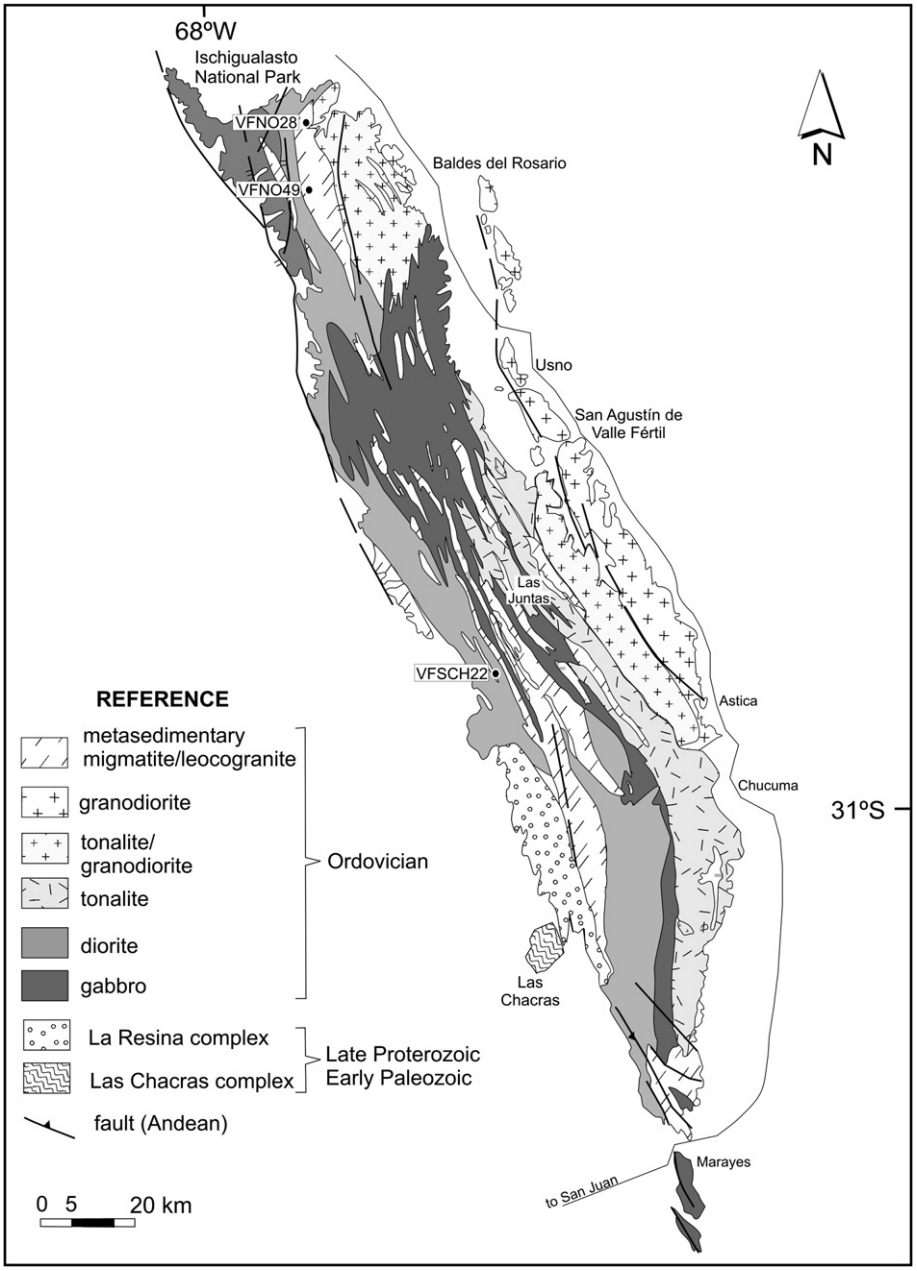

Fig. 2. Simplified geological map of the Sierras Valle Fértil–La Huerta taken after the geological maps of Mirré (1976), Vujovich et al. (1996) and Otamendi et al. (2009), showing the location of the areas where samples for this study were obtained.

craton-ward-dipping subduction zone is proposed to account for the Early Cambrian magmatic belt along the Gondwana border (Rapela et al., 1998; Schwartz et al., 2008; Hongn et al., 2010).

In contrast, Ordovician magmatism was significantly more voluminous, the Early Ordovician arc was constructed outboard of the latest Neoproterozoic–Lower Cambrian Pampean orogen, as proved by the existence of Early Ordovician plutons intruded into Pampean sequences (Pankhurst et al., 1998; 2000).

Between 28° and 36° latitudes south latitudes, the Early Ordovician arc occupies a central position between Neoproterozoic–Early Cambrian Gondwanan orogenic belts and a Laurentia-derived microplate with Mesoproterozoic basement (Naipauer et al., 2010; Varela et al., 2011; and references therein). These continental-scale relationships were considered strong evidence that the Early Ordovician destructive margin of Gondwana (Famatinian segment) was shut by a continent-to-continent collision, which involved a rapid shift from subduction-related arc system to mountain-building collisional orogen (Astini and Dávila, 2004; Ramos, 2004). Sedimentological, paleontological and stratigraphic observations as well as a large geochronological database indicate that the collision between the allochthonous Laurentia microplate (Precordillera/Cuyania terrane) and the once active Gondwana margin began in late Middle Ordovician time and lasted until late Silurian time (Astini and Dávila, 2004; Benedetto, 2004; Castro de Machuca et al., 2008; Gallien et al., 2010; Varela et al., 2011).

The Ordovician Famatinian orogenic system can be separated into two distinct provinces. The eastern province is dominated by Cambrian–Ordovician turbidite successions and their Early Ordovician metamorphic equivalents. These rocks were deposited in large basins between the Early Cambrian Pampean orogen and the proto-Pacific oceanic plates (Benedetto, 2004) and later underwent back-arc extension during the construction of the Early Ordovician arc (Astini and Dávila, 2004; Büttner et al., 2005; Larrovere et al., 2011). Like the eastern section, the western province also contains Cambrian–Ordovician turbidite successions, but it differs in that it is dominated by plutonic, volcanic and volcaniclastic rocks generated at the Early Ordovician active margin (Mannheim and Miller, 1996; Bahlburg, 1998; Bahlburg and Hervé, 1997; Coira et al., 1999; Astini, 2003).

The basement that underlies the Middle Cambrian–Ordovician turbidite successions is unknown. Because Middle Cambrian sediments uncomformably overlie folded Neoproterozoic to Lower Cambrian turbidite units of the Puncoviscana Formation, one possibility is that Neoproterozoic–Cambrian successions may underlie younger sedimentary sequences (Piñán-Llamas and Simpson, 2006). An alternative view is that Middle–Upper Cambrian sedimentary successions, which were deposited outboard of West Gondwana landmasses, might have been deposited upon Mesoproterozoic cratonized crust (e.g., Collo et al., 2009, and references therein). One point of agreement is that all these sedimentary successions were deposited along the edge of Gondwana, although at different distances from the continental margin.

3. Sampling rationale and specimen description

Metamorphic mineral assemblages and the most plausible protolith of samples chosen for U–Pb zircon geochronology are summarized in Table 1. Sample VFSCH22 was collected from the hanging wall of a Cenozoic fault that bounds the crystalline western side of the Sierra de Valle Fértil; it is also close to the paleo-suture zone buried by the Bermejo Valley (Fig. 2; Comínguez and Ramos, 1991). Samples VFNO49 and VFNO28 were taken from the

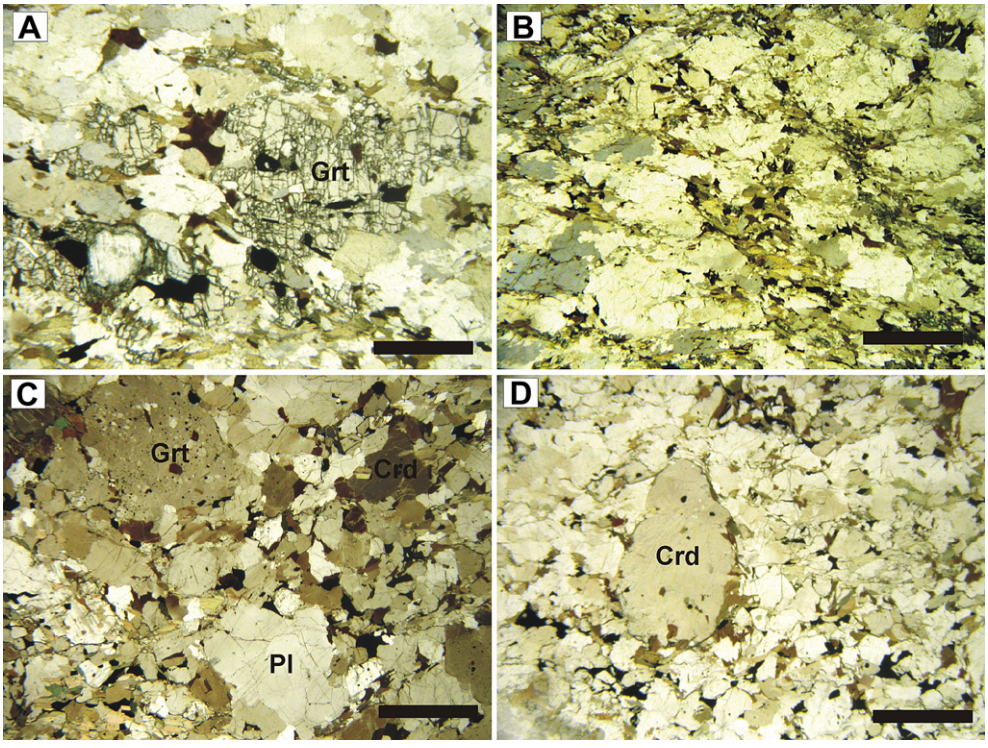

Fig. 3. Photomicrographs of the granulite–facies metasedimentary chosen to obtain detrital zircon ages. (A) Illustration of inequigranular interlobate texture of sample VFSCH22 consisting of quartz and plagioclase aggregates with subordinate biotite laths. The aggregate defines a foliation that wraps around strongly resorbed garnet porphyroblast. (B) In specimen VFSCH22, biotite-rich domains develop discontinuous schistosity with local crenulation cleavage, as observed in the S-shaped biotite aggregate at the centre of the image. (C) Seriate pseudo-polygonal fabric that dominates sample VFNO49, showing the coexistence of the peak mineral assemblage defined by quartz, plagioclase, garnet, biotite, cordierite and oxides. (D) Porphyroblast of idioblastic cordierite contrasting with the matrix assemblage that consists of plagioclase, quartz and biotite as observed in sample VFNO28. Cordierite is locally pseudomorphed by biotite on its borders. In all the photomicrographs the long dimension of the black bar is about 1 mm.

Table 2
U–Pb (zircon) geochronologic analyses by Laser-Ablation Multicollector ICP Mass Spectrometry.

	Isotopic ratios										Apparent ages (Ma)								
	U, ppm	U/Th	$^{206}Pb^*/^{204}Pb$	$^{206}Pb^*/^{207}Pb^*$	±(%)	$^{207}Pb^*/^{235}U^*$	±(%)	$^{206}Pb^*/^{238}U$	±(%)	Error Corr.	$^{206}Pb^*/^{238}U^*$	±(Ma)	$^{207}Pb^*/^{235}U$	±(Ma)	$^{206}Pb^*/^{207}Pb^*$	±(Ma)	Best age (Ma)	(Ma)	Conc. (%)
Grain																			
Sample: VFSCH22																			
1	575	4.8	395272	7.8946	0.7	6.0636	6.6	0.3472	6.6	0.99	1921.1	109.8	1985.0	58.0	2052.2	12.6	2052.2	12.6	93.6
2	418	6.6	36322	17.5147	3.8	0.6457	4.8	0.0820	2.9	0.61	508.2	14.1	505.8	18.9	495.2	83.2	508.2	14.1	102.6
3	*338*	*13.6*	*24996*	*18.8729*	*3.4*	*0.4713*	*19.8*	*0.0645*	*19.5*	*0.98*	*403.0*	*76.1*	*392.1*	*64.4*	*328.2*	*77.9*	*403.0*	*76.1*	*NA*
4	258	3.3	45988	13.5029	3.3	1.7653	5.2	0.1729	4.0	0.77	1028.0	38.1	1032.8	33.6	1043.0	66.2	1043.0	66.2	98.6
5	1108	63.2	159189	16.3988	2.2	0.8657	5.8	0.1030	5.4	0.93	631.8	32.5	633.2	27.5	638.5	47.4	631.8	32.5	98.9
5	186	3.3	116589	7.9800	2.0	6.4242	6.9	0.3718	6.6	0.96	2037.9	116.0	2035.6	61.1	2033.2	36.2	2033.2	36.2	100.2
7	*138*	*2.9*	*56439*	*14.4353*	*5.6*	*1.5759*	*7.3*	*0.1650*	*4.7*	*0.64*	*984.5*	*42.8*	*960.8*	*45.3*	*906.9*	*115.0*	*906.9*	*115.0*	*108.6*
8	314	2.4	5299	15.9544	13.3	0.7246	13.9	0.0838	3.9	0.28	519.1	19.2	553.4	59.2	697.3	285.0	519.1	19.2	74.4
9	*264*	*39.7*	*28155*	*18.8868*	*7.7*	*0.5235*	*8.8*	*0.0717*	*4.4*	*0.49*	*446.5*	*18.8*	*427.5*	*30.8*	*326.5*	*174.1*	*446.5*	*18.8*	*NA*
10	*257*	*14.0*	*23245*	*17.8006*	*6.3*	*0.5892*	*7.5*	*0.0761*	*4.1*	*0.55*	*472.6*	*18.8*	*470.4*	*28.2*	*459.4*	*139.0*	*472.6*	*18.8*	*NA*
11	571	4.2	202249	13.4525	1.2	1.8330	6.3	0.1788	6.2	0.98	1060.6	60.5	1057.4	41.4	1050.6	24.3	1050.6	24.3	101.0
12	442	5.6	4813	11.8973	15.1	1.7682	17.3	0.1526	8.6	0.50	915.4	73.3	1033.9	112.9	1293.8	294.6	1293.8	294.6	70.8
13	*334*	*27.3*	*33542*	*17.3432*	*5.0*	*0.5788*	*17.2*	*0.0728*	*16.5*	*0.96*	*453.1*	*72.0*	*463.7*	*64.1*	*516.8*	*109.4*	*453.1*	*72.0*	*NA*
14	*296*	*16.1*	*22249*	*18.8481*	*10.3*	*0.5395*	*10.9*	*0.0738*	*3.5*	*0.32*	*458.7*	*15.4*	*438.1*	*38.7*	*331.2*	*234.0*	*458.7*	*15.4*	*NA*
15	*374*	*4.8*	*55540*	*18.0610*	*7.9*	*0.5684*	*10.1*	*0.0745*	*6.4*	*0.63*	*462.9*	*28.4*	*457.0*	*37.2*	*427.1*	*175.7*	*462.9*	*28.4*	*NA*
16	*499*	*15.3*	*142699*	*17.2635*	*5.4*	*0.5914*	*9.2*	*0.0740*	*7.5*	*0.81*	*460.5*	*33.3*	*471.7*	*34.9*	*527.0*	*119.1*	*460.5*	*33.3*	*NA*
17	*288*	*5.0*	*2021*	*14.9867*	*15.3*	*0.7511*	*18.8*	*0.0816*	*11.0*	*0.58*	*505.9*	*53.3*	*568.8*	*82.1*	*829.3*	*320.6*	*505.9*	*53.3*	*61.0*
18	304	2.7	45446	13.6211	3.8	1.7763	4.8	0.1755	2.9	0.61	1042.2	28.2	1036.8	31.1	1025.4	76.7	1025.4	76.7	101.6
19	824	2.6	80370	13.2955	1.4	1.7988	6.1	0.1735	6.0	0.97	1031.1	56.9	1045.0	40.1	1074.2	28.1	1074.2	28.1	96.0
20	385	6.5	86167	14.3951	1.8	1.3600	4.0	0.1420	3.5	0.89	855.9	28.4	871.9	23.2	912.7	36.7	912.7	36.7	93.8
21	764	6.9	152800	13.9782	1.1	1.4947	3.2	0.1515	3.0	0.94	909.5	25.3	928.2	19.2	972.9	21.6	972.9	21.6	93.5
22	*186*	*3.0*	*13572*	*18.4016*	*14.7*	*0.6270*	*15.4*	*0.0837*	*4.3*	*0.28*	*518.0*	*21.4*	*494.2*	*60.2*	*385.3*	*332.7*	*518.0*	*21.4*	*NA*
23	175	4.2	42577	13.0952	3.9	1.8607	5.1	0.1767	3.3	0.65	1049.1	32.1	1067.2	33.7	1104.6	77.6	1104.6	77.6	95.0
24	177	2.2	140416	8.7764	1.8	4.9571	6.0	0.3155	5.7	0.95	1767.9	88.2	1812.0	50.5	1863.2	32.0	1863.2	32.0	94.9
25	*129*	*2.6*	*25206*	*16.3584*	*21.2*	*0.7951*	*29.2*	*0.0943*	*20.0*	*0.69*	*581.1*	*111.3*	*594.1*	*131.9*	*643.9*	*460.6*	*581.1*	*111.3*	*90.3*
26	247	33.1	168637	8.6937	2.3	4.7135	4.2	0.2972	3.5	0.83	1677.4	52.2	1769.6	35.5	1880.3	42.0	1880.3	42.0	89.2
27	493	7.7	82553	16.6169	3.8	0.7786	5.4	0.0938	3.8	0.70	578.2	20.8	584.7	23.8	610.0	82.2	578.2	20.8	94.8
28	*97*	*1.1*	*13615*	*17.9176*	*18.4*	*0.7718*	*19.5*	*0.1003*	*6.5*	*0.33*	*616.1*	*38.0*	*580.8*	*86.4*	*444.8*	*411.8*	*616.1*	*38.0*	*138.5*
30	*242*	*6.9*	*34474*	*16.4069*	*22.3*	*0.5350*	*23.2*	*0.0637*	*6.4*	*0.28*	*397.9*	*24.7*	*435.1*	*82.2*	*637.5*	*484.7*	*397.9*	*24.7*	*62.4*
31	118	1.3	71513	5.6471	1.0	11.1721	5.6	0.4576	5.5	0.98	2428.8	112.2	2537.6	52.5	2625.7	16.4	2625.7	16.4	92.5
32	223	0.9	28157	16.9430	7.0	0.7402	8.4	0.0910	4.6	0.55	561.2	24.8	562.5	36.3	567.9	152.9	561.2	24.8	98.8
33	248	0.7	71264	16.7493	4.0	0.8135	6.4	0.0988	5.0	0.78	607.5	28.8	604.4	29.0	592.8	85.8	607.5	28.8	102.5
34	157	5.5	38424	13.8172	5.7	1.6538	11.9	0.1657	10.4	0.88	988.6	95.6	991.0	75.4	996.5	115.9	996.5	115.9	99.2
35	1194	4.4	157333	16.3877	1.4	0.8228	2.8	0.0978	2.4	0.86	601.4	14.0	609.6	12.9	640.0	30.7	601.4	14.0	94.0
36	849	13.9	406224	14.7069	1.6	1.1241	3.5	0.1199	3.0	0.88	730.0	21.0	764.9	18.6	868.4	34.0	730.0	21.0	84.1
37	364	3.8	34728	16.2737	5.1	0.8065	8.4	0.0952	6.6	0.79	586.2	36.9	600.5	37.9	655.0	110.3	586.2	36.9	89.5
38	*314*	*17.3*	*37588*	*17.9771*	*9.2*	*0.5651*	*9.6*	*0.0737*	*2.8*	*0.30*	*458.3*	*12.6*	*454.8*	*35.2*	*437.5*	*204.2*	*458.3*	*12.6*	*NA*
39	670	20.4	105249	13.6796	3.9	1.4284	8.9	0.1417	8.0	0.90	854.3	64.0	900.9	53.2	1016.7	79.0	1016.7	79.0	84.0
40	390	4.4	135700	13.4603	2.8	1.8158	4.9	0.1773	4.0	0.82	1052.0	38.9	1051.2	32.1	1049.4	56.8	1049.4	56.8	100.2
41	*457*	*3.9*	*66274*	*15.6796*	*7.5*	*0.6720*	*19.2*	*0.0764*	*17.7*	*0.92*	*474.7*	*80.9*	*521.9*	*78.5*	*734.3*	*159.0*	*474.7*	*80.9*	*64.6*
42	356	1.4	113371	11.8216	1.1	2.5674	4.8	0.2201	4.7	0.97	1282.5	54.5	1291.4	35.2	1306.2	21.4	1306.2	21.4	98.2
43	*295*	*5.1*	*124349*	*12.5879*	*25.3*	*0.5261*	*61.3*	*0.0480*	*55.8*	*0.91*	*302.4*	*164.9*	*429.2*	*217.7*	*1183.2*	*507.2*	*302.4*	*164.9*	*25.6*
44	361	12.8	59431	16.7608	5.9	0.6078	10.8	0.0739	9.1	0.84	459.5	40.3	482.2	41.6	591.4	128.2	459.5	40.3	77.7
45	254	3.8	43547	16.9365	6.1	0.6895	7.6	0.0847	4.5	0.59	524.1	22.7	532.5	31.6	568.7	133.7	524.1	22.7	92.1
46	371	2.0	45133	16.8078	5.5	0.7236	7.2	0.0882	4.7	0.65	544.9	24.6	552.8	30.9	585.3	119.4	544.9	24.6	93.1
47	*294*	*2.6*	*31368*	*17.6776*	*9.7*	*0.6937*	*10.6*	*0.0889*	*4.4*	*0.41*	*549.2*	*23.1*	*535.0*	*44.2*	*474.7*	*214.5*	*549.2*	*23.1*	*115.7*
48	202	2.9	38926	13.3625	5.7	1.8338	28.2	0.1777	27.6	0.98	1054.5	268.6	1057.6	187.3	1064.1	115.5	1064.1	115.5	99.1
49	111	1.5	88820	10.8756	2.9	2.9899	4.2	0.2358	3.1	0.74	1365.0	38.4	1405.0	32.2	1466.3	54.4	1466.3	54.4	93.1
50	420	7.1	29162	15.7920	3.8	0.9060	4.9	0.1038	3.1	0.64	636.4	19.0	654.9	23.7	719.1	80.3	636.4	19.0	88.5
51	*145*	*2.7*	*144950*	*9.6074*	*3.8*	*2.6603*	*28.8*	*0.1854*	*28.6*	*0.99*	*1096.2*	*288.4*	*1317.5*	*216.0*	*1698.2*	*69.5*	*1698.2*	*69.5*	*64.6*
52	209	2.5	100407	8.0686	1.4	5.7413	5.5	0.3360	5.3	0.97	1867.3	85.6	1937.6	47.3	2013.7	24.7	2013.7	24.7	92.7

(*continued on next page*)

Table 2 (*continued*)

	Isotopic ratios										Apparent ages (Ma)								
	U, ppm	U/Th	$^{206}Pb^*/^{204}Pb$	$^{206}Pb^*/^{207}Pb^*$	±(%)	$^{207}Pb^*/^{235}U^*$	±(%)	$^{206}Pb^*/^{238}U$	±(%)	Error Corr.	$^{206}Pb^*/^{238}U^*$	±(Ma)	$^{207}Pb^*/^{235}U$	±(Ma)	$^{206}Pb^*/^{207}Pb^*$	±(Ma)	Best age (Ma)	(Ma)	Conc. (%)
53	*363*	*14.3*	*16102*	*15.9353*	*9.1*	*0.6198*	*10.7*	*0.0716*	*5.6*	*0.53*	*446.0*	*24.3*	*489.7*	*41.6*	*699.9*	*194.2*	*446.0*	*24.3*	*63.7*
54	*223*	*2.7*	*43819*	*17.6226*	*8.7*	*0.7153*	*10.1*	*0.0914*	*5.0*	*0.49*	*563.9*	*26.9*	*547.9*	*42.6*	*481.6*	*193.3*	*563.9*	*26.9*	*117.1*
55	*215*	*3.1*	*42654*	*16.7724*	*6.3*	*0.8300*	*11.0*	*0.1010*	*9.1*	*0.82*	*620.0*	*53.7*	*613.6*	*50.9*	*589.9*	*135.9*	*620.0*	*53.7*	*105.1*
56	168	2.7	20846	17.1374	16.9	0.6335	20.5	0.0787	11.6	0.56	488.6	54.4	498.3	80.8	543.0	372.1	488.6	54.4	90.0
57	652	8.6	41937	16.1911	4.9	0.8622	12.2	0.1012	11.2	0.92	621.7	66.4	631.3	57.5	665.9	104.3	621.7	66.4	93.4
58	*357*	*11.0*	*32231*	*16.8237*	*5.6*	*0.5616*	*36.4*	*0.0685*	*35.9*	*0.99*	*427.3*	*148.6*	*452.6*	*133.6*	*583.2*	*122.6*	*427.3*	*148.6*	*73.3*
59	202	3.3	85833	14.5032	8.4	1.4400	12.3	0.1515	9.1	0.73	909.2	76.8	905.7	74.0	897.2	172.8	897.2	172.8	101.3
60	551	3.2	171508	13.6889	4.0	1.6512	7.3	0.1639	6.1	0.83	978.6	55.0	990.0	46.0	1015.4	81.2	1015.4	81.2	96.4
61	226	1.2	24222	17.3601	8.4	0.6832	9.6	0.0860	4.6	0.48	531.9	23.3	528.7	39.5	514.7	185.4	531.9	23.3	103.3
62	*146*	*4.7*	*34165*	*16.2806*	*8.6*	*0.9744*	*11.2*	*0.1151*	*7.1*	*0.64*	*702.0*	*47.4*	*690.7*	*56.0*	*654.1*	*184.3*	*702.0*	*47.4*	*107.3*
63	199	2.3	35672	16.9620	9.3	0.7060	10.9	0.0869	5.7	0.52	536.9	29.3	542.4	45.8	565.4	202.5	536.9	29.3	95.0
64	*378.3*	*11.4*	*47120.8*	*17.2*	*5.8*	*0.6*	*9.8*	*0.1*	*7.8*	*0.8*	*464.6*	*35.1*	*476.4*	*37.2*	*533.4*	*127.9*	*464.6*	*35.1*	*NA*
65	*321*	*1.2*	*200761*	*9.4701*	*3.2*	*2.8599*	*8.4*	*0.1964*	*7.7*	*0.92*	*1156.1*	*81.9*	*1371.4*	*63.1*	*1724.7*	*59.1*	*1724.7*	*59.1*	*67.0*
66	317	1.7	34605	16.4412	7.7	0.7323	8.6	0.0873	3.9	0.45	539.7	20.3	557.9	37.1	633.0	165.8	539.7	20.3	85.3
67	562	2.7	201416	16.1763	3.7	0.8644	5.6	0.1014	4.2	0.75	622.7	25.0	632.5	26.3	667.8	78.6	622.7	25.0	93.2
68	155	0.7	19511	17.3751	13.5	0.6320	14.9	0.0796	6.2	0.42	494.0	29.6	497.3	58.7	512.8	298.8	494.0	29.6	96.3
69	270	2.1	110758	13.7852	4.0	1.5302	4.7	0.1530	2.5	0.52	917.7	21.2	942.6	29.0	1001.1	81.6	1001.1	81.6	91.7
70	*151*	*1.5*	*16146*	*18.2194*	*12.2*	*0.6863*	*13.6*	*0.0907*	*5.9*	*0.44*	*559.6*	*31.8*	*530.6*	*56.3*	*407.6*	*274.9*	*559.6*	*31.8*	*NA*
71	332	6.2	77129	15.6962	4.2	1.0731	6.5	0.1222	4.9	0.76	743.0	34.7	740.3	34.2	732.0	89.5	743.0	34.7	101.5
72	258	0.6	105103	13.4265	2.3	1.8019	3.8	0.1755	3.1	0.80	1042.1	29.5	1046.1	25.1	1054.5	46.6	1054.5	46.6	98.8
73	*140.4*	*0.7*	*17803.5*	*18.0*	*14.4*	*0.6*	*15.5*	*0.1*	*5.7*	*0.4*	*483.6*	*26.6*	*475.1*	*58.9*	*434.7*	*322.2*	*483.6*	*26.6*	*NA*
74	141	1.6	14060	16.0885	14.8	0.7581	18.0	0.0885	10.3	0.57	546.4	53.8	572.9	79.2	679.5	318.7	546.4	53.8	80.4
75	238	2.5	24543	16.3628	7.3	0.6987	9.4	0.0829	5.9	0.63	513.5	29.1	538.0	39.1	643.3	156.6	513.5	29.1	79.8
76	*320*	*30.9*	*39943*	*17.7630*	*8.3*	*0.5659*	*9.8*	*0.0729*	*5.2*	*0.53*	*453.6*	*22.9*	*455.4*	*36.1*	*464.1*	*184.8*	*453.6*	*22.9*	*NA*
77	197	1.5	26499	16.5473	10.2	0.6778	11.3	0.0813	4.9	0.44	504.1	24.0	525.4	46.4	619.1	219.9	504.1	24.0	81.4
78	*188*	*2.1*	*48113*	*18.1380*	*11.2*	*0.6153*	*12.5*	*0.0809*	*5.5*	*0.44*	*501.7*	*26.5*	*486.9*	*48.2*	*417.6*	*250.5*	*501.7*	*26.5*	*NA*
79	*180*	*51.7*	*14983.6*	*19.5*	*12.3*	*0.5104*	*15.7*	*0.0723*	*9.8*	*0.62*	*449.9*	*42.5*	*418.7*	*53.9*	*250.5*	*282.9*	*449.9*	*42.5*	*NA*
80	811	2.2	392083	5.8122	1.0	10.4497	4.8	0.4405	4.7	0.98	2352.9	92.7	2475.5	44.6	2577.7	16.6	2577.7	16.6	91.3
81	179	1.8	31040	18.0843	17.2	0.6479	18.6	0.0850	7.2	0.39	525.8	36.4	507.2	74.4	424.2	385.2	525.8	36.4	NA
82	413	1.1	157296	13.0658	1.9	1.8220	2.2	0.1727	1.1	0.52	1026.7	10.7	1053.4	14.3	1109.1	37.3	1109.1	37.3	92.6
83	*91*	*1.6*	*14646*	*19.2381*	*29.6*	*0.6027*	*30.4*	*0.0841*	*6.8*	*0.22*	*520.5*	*34.1*	*478.9*	*116.5*	*284.6*	*690.7*	*520.5*	*34.1*	*NA*
84	270	2.3	77227	13.7238	3.1	1.6286	6.0	0.1621	5.2	0.86	968.4	46.4	981.3	38.0	1010.2	63.3	1010.2	63.3	95.9
85	304	3.0	34737	17.2257	6.9	0.6534	9.5	0.0816	6.5	0.68	505.9	31.5	510.6	38.1	531.8	152.2	505.9	31.5	95.1
86	214	5.0	35116	16.9427	7.5	0.6060	9.2	0.0745	5.3	0.58	463.0	23.7	481.0	35.2	568.0	163.1	463.0	23.7	81.5
87	213	5.0	45785	16.7774	10.6	0.6212	12.4	0.0756	6.5	0.52	469.7	29.2	490.6	48.3	589.2	230.3	469.7	29.2	79.7
88	321	2.9	77791	13.6202	3.9	1.5487	9.7	0.1530	8.9	0.92	917.7	75.8	950.0	59.7	1025.6	78.6	1025.6	78.6	89.5
89	962	4.8	36559	14.4363	1.8	1.2345	8.9	0.1293	8.7	0.98	783.6	64.5	816.4	50.2	906.8	37.9	906.8	37.9	86.4
90	176	1.5	24967	17.1027	12.8	0.6541	15.7	0.0811	9.1	0.58	502.9	44.3	511.0	63.1	547.4	279.9	502.9	44.3	91.9
91	832	23.6	181902	13.7171	1.2	1.5529	4.1	0.1545	3.9	0.96	926.1	33.7	951.6	25.2	1011.2	24.4	1011.2	24.4	91.6
92	*182*	*55.0*	*37325*	*18.1739*	*12.6*	*0.5534*	*13.6*	*0.0729*	*4.9*	*0.36*	*453.9*	*21.6*	*447.2*	*49.1*	*413.2*	*283.7*	*453.9*	*21.6*	*NA*
93	468	5.9	83701	15.6891	3.1	1.0824	8.8	0.1232	8.3	0.94	748.7	58.4	744.8	46.6	733.0	65.8	748.7	58.4	102.1
94	*252*	*22.0*	*592*	*10.7993*	*8.6*	*1.5260*	*9.2*	*0.1195*	*3.2*	*0.35*	*727.8*	*21.9*	*940.9*	*56.2*	*1479.7*	*163.1*	*1479.7*	*163.1*	*49.2*
95	*321*	*6.8*	*96309*	*11.4215*	*22.0*	*1.5341*	*37.4*	*0.1271*	*30.3*	*0.81*	*771.2*	*220.2*	*944.1*	*234.0*	*1372.7*	*427.9*	*1372.7*	*427.9*	*56.2*
96	*172*	*3.1*	*5882*	*14.9328*	*11.0*	*0.7181*	*16.7*	*0.0778*	*12.5*	*0.75*	*482.8*	*58.0*	*549.5*	*70.8*	*836.8*	*230.7*	*482.8*	*58.0*	*57.7*
97	*258*	*1.4*	*54920*	*17.9035*	*9.4*	*0.6150*	*11.2*	*0.0799*	*6.1*	*0.54*	*495.3*	*28.9*	*486.7*	*43.2*	*446.6*	*209.0*	*495.3*	*28.9*	*NA*
98	273	2.4	76239	12.7350	1.2	1.9238	2.7	0.1777	2.4	0.89	1054.4	23.5	1089.4	18.1	1160.1	24.4	1160.1	24.4	90.9
99	*314*	*1.2*	*30976*	*17.5821*	*7.0*	*0.6560*	*8.0*	*0.0836*	*4.0*	*0.49*	*517.9*	*19.8*	*512.2*	*32.4*	*486.7*	*154.5*	*517.9*	*19.8*	*106.4*
100	*71*	*1.3*	*8386*	*14.8000*	*29.8*	*0.8505*	*34.2*	*0.0913*	*16.9*	*0.49*	*563.2*	*91.3*	*624.9*	*161.1*	*855.3*	*631.4*	*563.2*	*91.3*	*65.8*
Sample: VFNO28																			
1	1.1	0.6	67653	16.5949	3.3	0.8158	5.7	0.0982	4.7	0.82	603.7	26.9	605.7	26.1	612.9	71.5	603.7	26.9	98.5
2	4.1	1.5	28205	16.4093	6.4	0.8615	8.3	0.1025	5.3	0.63	629.2	31.6	630.9	39.2	637.2	138.8	629.2	31.6	98.7
3	3.0	*4.0*	*15078*	*17.1600*	*8.6*	*0.8284*	*9.3*	*0.1031*	*3.5*	*0.38*	*632.6*	*21.1*	*612.7*	*42.7*	*540.1*	*188.4*	*632.6*	*21.1*	*117.1*
4	1.8	1.2	65159	8.1657	1.5	6.2410	9.0	0.3696	8.9	0.99	2027.6	155.0	2010.2	79.2	1992.4	26.4	1992.4	26.4	101.8
5	0.6	2.0	87972	13.3115	3.2	1.7308	8.3	0.1671	7.7	0.92	996.1	70.9	1020.1	53.6	1071.8	64.6	1071.8	64.6	92.9

6	1.6	1.2	26934	13.3131	6.5	1.7223	9.7	0.1663	7.2	0.74	991.7	66.3	1016.9	62.5	1071.6	131.1	1071.6	131.1	92.5
8	3.0	2.5	47295	15.2783	9.4	0.8570	27.7	0.0950	26.1	0.94	584.8	145.8	628.5	131	788.9	198.3	584.8	145.8	74.1
9	1.7	0.8	29548	14.1792	7.9	1.5478	8.4	0.1592	2.7	0.33	952.2	24.3	949.6	51.6	943.7	161.8	943.7	161.8	100.9
10	1.6	2.4	83166	13.6310	5.6	1.8420	6.7	0.1821	3.8	0.56	1078.5	37.7	1060.6	44.4	1023.9	112.7	1023.9	112.7	105.3
11	2.6	1.7	63906	15.9535	3.3	0.8190	4.5	0.0948	3.1	0.67	583.7	17.1	607.5	20.7	697.5	71.4	583.7	17.1	83.7
12	1.3	*1.7*	*14532*	*14.4475*	*31.6*	*0.8174*	*32.4*	*0.0857*	*7.2*	*0.22*	*529.8*	*36.9*	*606.6*	*148.9*	*905.2*	*666.3*	*529.8*	*36.9*	*58.5*
13	2.6	1.6	35147	12.5809	4.0	1.8568	5.7	0.1694	4.1	0.71	1008.9	37.9	1065.8	37.7	1184.3	79.2	1184.3	79.2	85.2
14	0.9	1.4	52348	17.4169	6.9	0.6448	8.2	0.0814	4.4	0.53	504.8	21.1	505.3	32.6	507.5	152.5	504.8	21.1	99.5
15	1.2	2.3	42662	13.0956	6.0	1.7386	7.6	0.1651	4.6	0.61	985.2	41.9	1022.9	48.9	1104.6	120.7	1104.6	120.7	89.2
16	1.3	*1.7*	*5760*	*6.1275*	*250*	*1.7887*	*251*	*0.0795*	*15.3*	*0.06*	*493.1*	*72.7*	*1041.3*		*2489.0*	*14.1*	*2489.0*	*14.1*	*19.8*
17	9.5	0.7	3385	16.1258	52.2	0.8560	52.9	0.1001	8.9	0.17	615.1	52.3	628.0	253.0	674.5	1198	615.1	52.3	91.2
18	0.5	2.0	24844	14.2440	9.3	1.4601	11.6	0.1508	6.9	0.60	905.6	58.7	914.0	69.9	934.4	190.4	934.4	190.4	96.9
19	0.9	*1.5*	*19458*	*23.1137*	*61.2*	*0.4829*	*61.3*	*0.0810*	*3.8*	*0.06*	*501.9*	*18.2*	*400.1*	*205.6*	*-152.4*	*1671*	*501.9*	*18.2*	*NA*
20	2.2	1.6	97194	15.9614	6.2	0.7396	6.9	0.0856	3.0	0.44	529.6	15.4	562.2	29.8	696.4	132.3	529.6	15.4	76.0
21	1.0	0.9	53550	16.3765	5.4	0.9284	6.3	0.1103	3.3	0.52	674.3	21.3	666.8	31.0	641.5	116.1	674.3	21.3	105.1
22	0.7	*1.9*	*18236*	*19.1023*	*21.4*	*0.6446*	*22.2*	*0.0893*	*5.9*	*0.27*	*551.4*	*31.2*	*505.1*	*88.6*	*300.7*	*493.4*	*551.4*	*31.2*	*NA*
23	2.2	1.8	120933	10.3775	1.9	3.5865	4.9	0.2699	4.5	0.92	1540.5	62.0	1546.5	39.1	1554.8	36.0	1554.8	36.0	99.1
24	4.7	*1.1*	*171050*	*12.9983*	*1.3*	*2.1653*	*2.0*	*0.2041*	*1.6*	*0.77*	*1197.5*	*17.1*	*1170.0*	*14.1*	*1119.5*	*25.8*	*1119.5*	*25.8*	*107.0*
25	1.2	*29.5*	*31400*	*15.2088*	*10.7*	*1.4837*	*26.9*	*0.1637*	*24.7*	*0.92*	*977.1*	*223.8*	*923.7*	*164.6*	*798.5*	*225.0*	*977.1*	*223.8*	*122.4*
26	5.1	*1.4*	*23887*	*15.2098*	*17.3*	*0.7137*	*18.4*	*0.0787*	*6.4*	*0.35*	*488.6*	*30.1*	*547.0*	*78.1*	*798.3*	*365.0*	*488.6*	*30.1*	*61.2*
27	1.2	*2.6*	*13671*	*18.0745*	*25.0*	*0.6377*	*25.9*	*0.0836*	*6.7*	*0.26*	*517.5*	*33.3*	*500.9*	*102.8*	*425.4*	*566.3*	*517.5*	*33.3*	*NA*
28	1.5	4.5	55262	16.2488	5.5	0.9117	6.1	0.1074	2.8	0.46	657.8	17.5	657.9	29.7	658.3	117.1	657.8	17.5	99.9
29	2.2	2.3	53197	16.9691	4.9	0.7052	5.1	0.0868	1.4	0.28	536.5	7.4	541.9	21.5	564.5	107.2	536.5	7.4	95.0
30	1.9	0.8	27285	8.6108	5.7	5.2163	8.2	0.3258	6.0	0.72	1817.8	94.6	1855.3	70.3	1897.5	102.2	1897.5	102.2	95.8
31	1.2	1.7	46110	16.0246	11.8	0.7311	13.8	0.0850	7.2	0.52	525.7	36.2	557.2	59.2	688.0	252.2	525.7	36.2	76.4
32	9.0	*2.0*	*12623*	*17.6677*	*13.1*	*0.6190*	*15.9*	*0.0793*	*9.1*	*0.57*	*492.1*	*42.9*	*489.2*	*61.8*	*476.0*	*290.4*	*492.1*	*42.9*	*NA*
33	0.9	5.2	52408	15.8119	3.6	0.9923	4.4	0.1138	2.6	0.59	694.8	17.0	699.9	22.3	716.4	75.7	694.8	17.0	97.0
34	1.6	1.3	137890	14.8395	1.7	1.3326	7.1	0.1434	6.9	0.97	864.0	55.6	860.0	41.0	849.8	34.6	864.0	55.6	101.7
35	5.8	*1.8*	*20899*	*17.4311*	*12.7*	*0.6891*	*12.9*	*0.0871*	*2.4*	*0.19*	*538.4*	*12.6*	*532.2*	*53.6*	*505.8*	*280.2*	*538.4*	*12.6*	*106.5*
36	2.7	5.8	31406	16.8444	5.0	0.7541	7.6	0.0921	5.7	0.75	568.1	30.7	570.6	33.0	580.6	109.1	568.1	30.7	97.8
37	3.0	1.8	53258	13.1239	3.8	1.7754	5.3	0.1690	3.7	0.70	1006.6	34.8	1036.5	34.4	1100.3	75.3	1100.3	75.3	91.5
38	2.6	2.2	32115	17.1846	10.5	0.6728	10.7	0.0839	2.3	0.21	519.1	11.5	522.4	43.8	537.0	229.4	519.1	11.5	96.7
39	4.4	*4.0*	*42578*	*17.6324*	*6.5*	*0.6821*	*6.8*	*0.0872*	*2.0*	*0.29*	*539.2*	*10.2*	*528.1*	*28.0*	*480.4*	*144.0*	*539.2*	*10.2*	*112.2*
40	3.0	*9.8*	*64228*	*17.6377*	*4.3*	*0.5940*	*5.0*	*0.0760*	*2.6*	*0.52*	*472.1*	*12.0*	*473.4*	*19.0*	*479.7*	*94.3*	*472.1*	*12.0*	*NA*
41	1.5	3.7	208041	13.4549	1.9	1.6802	3.7	0.1640	3.1	0.85	978.7	28.5	1001.0	23.5	1050.2	38.9	1050.2	38.9	93.2
42	4.6	2.1	86721	8.3220	1.1	5.7300	13.9	0.3458	13.9	1.00	1914.7	229.9	1935.9	120.9	1958.6	20.5	1958.6	20.5	97.8
43	2.0	*1.6*	*18619*	*17.7471*	*15.7*	*0.6625*	*18.4*	*0.0853*	*9.6*	*0.52*	*527.5*	*48.9*	*516.2*	*74.7*	*466.1*	*349.7*	*527.5*	*48.9*	*NA*
44	1.5	2.8	30658	16.9004	10.8	0.6389	11.2	0.0783	2.9	0.26	486.0	13.6	501.6	44.3	573.4	235.3	486.0	13.6	84.8
45	1.8	*2.4*	*82672*	*13.5328*	*1.9*	*1.9269*	*5.8*	*0.1891*	*5.5*	*0.94*	*1116.6*	*56.5*	*1090.5*	*39.0*	*1038.6*	*39.1*	*1038.6*	*39.1*	*107.5*
46	1.6	1.5	100557	13.2396	2.0	1.8230	3.1	0.1751	2.3	0.75	1039.9	22.2	1053.8	20.3	1082.7	41.0	1082.7	41.0	96.1
47	1.4	1.9	33979	16.8802	5.3	0.7123	6.9	0.0872	4.5	0.65	539.0	23.3	546.1	29.2	575.9	114.3	539.0	23.3	93.6
48	1.3	2.4	196610	8.6248	2.3	4.9408	4.7	0.3091	4.1	0.87	1736.1	62.7	1809.2	39.9	1894.6	41.5	1894.6	41.5	91.6
49	2.2	2.6	49606	12.8137	6.1	1.8710	8.8	0.1739	6.4	0.72	1033.5	60.8	1070.9	58.6	1147.9	122.0	1147.9	122.0	90.0
50	1.6	1.1	103934	15.8866	2.8	0.8596	4.8	0.0990	3.8	0.81	608.8	22.3	629.9	22.3	706.4	59.9	608.8	22.3	86.2
51	5.3	*2.6*	*224359*	*16.2776*	*4.6*	*0.9659*	*5.0*	*0.1140*	*1.9*	*0.38*	*696.1*	*12.5*	*686.3*	*24.9*	*654.5*	*99.0*	*696.1*	*12.5*	*106.4*
52	13.0	1.6	37364	17.5412	18.0	0.6504	18.4	0.0827	3.9	0.21	512.5	19.2	508.7	73.9	491.9	400.5	512.5	19.2	104.2
53	1.2	0.9	11257	15.4127	16.6	0.8053	17.6	0.0900	5.9	0.33	555.7	31.2	599.8	79.9	770.5	351.6	555.7	31.2	72.1
54	0.8	*1.6*	*12677*	*19.8257*	*17.8*	*0.6580*	*19.5*	*0.0946*	*8.0*	*0.41*	*582.8*	*44.4*	*513.4*	*78.7*	*215.3*	*414.8*	*582.8*	*44.4*	*NA*
55	1.1	0.5	52861	12.9367	6.7	1.9414	8.3	0.1821	4.9	0.59	1078.7	48.9	1095.5	56.0	1128.9	134.4	1128.9	134.4	95.6
56	2.2	1.4	40906	13.1348	2.6	1.8220	6.5	0.1736	6.0	0.92	1031.7	56.9	1053.4	42.8	1098.6	52.4	1098.6	52.4	93.9
57	1.9	2.9	114271	16.2751	6.5	0.8037	8.2	0.0949	4.9	0.60	584.3	27.3	598.9	36.9	654.8	140.0	584.3	27.3	89.2
58	5.1	1.7	39846	17.1160	8.3	0.6650	9.8	0.0825	5.1	0.52	511.3	25.1	517.6	39.7	545.7	182.7	511.3	25.1	93.7
59	0.8	1.0	99019	13.3905	3.7	1.8458	4.5	0.1793	2.6	0.57	1063.0	25.3	1062.0	29.9	1059.9	75.1	1059.9	75.1	100.3
60	1.6	1.7	21479	17.4290	8.2	0.6826	9.2	0.0863	4.1	0.45	533.6	21.0	528.4	37.9	506.0	181.4	533.6	21.0	105.4
60	1.2	5.0	178328	17.2742	5.4	0.7194	7.1	0.0901	4.6	0.65	556.3	24.7	550.3	30.2	525.6	118.7	556.3	24.7	105.8
61	3.5	3.3	65394	13.6090	2.3	1.7999	3.6	0.1777	2.8	0.77	1054.1	27.5	1045.4	23.8	1027.2	46.6	1027.2	46.6	102.6
62	6.8	2.5	133610	11.9201	2.1	2.4462	4.7	0.2115	4.2	0.89	1236.7	46.8	1256.3	33.6	1290.0	40.8	1290.0	40.8	95.9
63	1.3	1.6	49798	13.3047	4.6	1.7742	5.2	0.1712	2.5	0.48	1018.7	23.8	1036.1	34.0	1072.8	92.2	1072.8	92.2	95.0
64	7.0	*1.7*	*43054*	*17.9213*	*14.7*	*0.5926*	*17.1*	*0.0770*	*8.7*	*0.51*	*478.3*	*40.2*	*472.5*	*64.6*	*444.4*	*327.7*	*478.3*	*40.2*	*NA*

(*continued on next page*)

Table 2 (*continued*)

	Isotopic ratios										Apparent ages (Ma)								
	U, ppm	U/Th	$^{206}Pb^*/^{204}Pb$	$^{206}Pb^*/^{207}Pb^*$	±(%)	$^{207}Pb^*/^{235}U^*$	±(%)	$^{206}Pb^*/^{238}U$	±(%)	Error Corr.	$^{206}Pb^*/^{238}U^*$	±(Ma)	$^{207}Pb^*/^{235}U$	±(Ma)	$^{206}Pb^*/^{207}Pb^*$	±(Ma)	Best age (Ma)	(Ma)	Conc. (%)
65	2.6	1.5	38759	17.1611	4.5	0.6772	9.9	0.0843	8.9	0.89	521.6	44.4	525.1	40.8	540.0	99.1	521.6	44.4	96.6
66	2.4	1.8	59418	14.0864	5.0	1.4183	10.0	0.1449	8.7	0.86	872.3	70.7	896.6	59.7	957.1	103.1	957.1	103.1	91.1
67	2.0	4.6	74194	15.0473	4.2	1.1080	7.9	0.1209	6.7	0.85	735.9	46.8	757.2	42.4	820.8	88.1	735.9	46.8	89.6
68	1.1	1.1	36733	17.0850	10.5	0.7006	12.6	0.0868	7.0	0.55	536.6	35.8	539.1	52.7	549.7	229.8	536.6	35.8	97.6
69	1.0	0.4	78919	9.3266	4.3	4.2334	6.0	0.2864	4.2	0.70	1623.3	60.2	1680.5	49.3	1752.7	78.4	1752.7	78.4	92.6
70	0.8	1.3	68198	16.2068	5.2	0.9506	7.7	0.1117	5.6	0.73	682.8	36.4	678.4	37.9	663.8	111.8	682.8	36.4	102.9
71	2.0	0.4	52106	16.9014	4.0	0.7531	8.9	0.0923	7.9	0.89	569.2	43.0	570.0	38.7	573.3	87.5	569.2	43.0	99.3
72	1.4	1.4	168948	17.2851	1.8	0.7293	8.9	0.0914	8.8	0.98	564.0	47.3	556.2	38.3	524.2	39.4	564.0	47.3	107.6
73	2.3	*6.5*	*68662*	*8.7677*	*12.6*	*6.1441*	*31.9*	*0.3907*	*29.4*	*0.92*	*2126.1*	*532.8*	*1996.5*	*286.2*	*1865.0*	*228.0*	*1865.0*	*228.0*	*114.0*
74	1.4	2.2	19831	14.0999	10.9	1.1854	12.3	0.1212	5.7	0.46	737.6	39.7	793.8	67.7	955.2	223.1	737.6	39.7	77.2
75	1.0	*1.3*	*42713*	*13.6444*	*3.9*	*1.8932*	*5.8*	*0.1874*	*4.3*	*0.74*	*1107.0*	*44.1*	*1078.7*	*38.9*	*1022.0*	*79.3*	*1022.0*	*79.3*	*108.3*
76	2.3	1.8	68022	15.6531	4.1	1.1083	5.6	0.1258	3.8	0.69	764.0	27.6	757.3	29.8	737.8	85.8	764.0	27.6	103.5
77	1.6	2.9	205863	6.1254	1.0	9.4791	2.6	0.4211	2.4	0.92	2265.5	45.6	2385.5	23.8	2489.6	17.1	2489.6	17.1	91.0
78	2.8	1.0	38010	15.6036	11.3	0.7208	11.7	0.0816	3.1	0.26	505.5	15.1	551.1	50.0	744.5	240.1	505.5	15.1	67.9
79	2.1	1.7	48356	13.6250	1.7	1.7839	2.3	0.1763	1.5	0.68	1046.6	14.8	1039.6	14.7	1024.9	33.8	1024.9	33.8	102.1
80	1.7	3.2	21171	16.9489	5.9	0.6192	10.1	0.0761	8.3	0.82	472.9	37.8	489.3	39.4	567.1	127.8	472.9	37.8	83.4
81	2.6	2.8	657030	5.9828	0.3	10.6226	2.8	0.4609	2.8	0.99	2443.7	56.2	2490.7	25.8	2529.2	5.6	2529.2	5.6	96.6
82	2.4	0.8	78647	5.7511	1.4	11.2049	2.4	0.4674	2.0	0.82	2472.0	41.2	2540.3	22.8	2595.3	23.4	2595.3	23.4	95.2
83	1.1	6.1	42339	16.9471	6.8	0.6415	13.0	0.0788	11.1	0.85	489.2	52.2	503.2	51.7	567.4	148.7	489.2	52.2	86.2
84	1.0	2.3	19817	13.5325	5.2	1.8102	6.6	0.1777	4.0	0.61	1054.2	38.8	1049.1	43.0	1038.6	105.4	1038.6	105.4	101.5
85	0.5	*1.0*	*47486*	*17.3704*	*11.7*	*0.6953*	*12.8*	*0.0876*	*5.0*	*0.39*	*541.3*	*25.9*	*536.0*	*53.2*	*513.4*	*258.8*	*541.3*	*25.9*	*105.4*
86	1.3	*1.1*	*8510*	*16.8689*	*6.7*	*0.8384*	*9.4*	*0.1026*	*6.6*	*0.70*	*629.5*	*39.7*	*618.3*	*43.5*	*577.4*	*144.8*	*629.5*	*39.7*	*109.0*
87	0.6	4.1	87265	17.2029	9.5	0.6823	10.2	0.0851	3.8	0.37	526.7	19.3	528.2	42.1	534.6	207.8	526.7	19.3	98.5
88	1.5	16.0	106205	16.4755	3.6	0.8237	6.0	0.0984	4.8	0.80	605.2	27.7	610.1	27.4	628.5	76.5	605.2	27.7	96.3
89	2.4	*1.8*	*68262*	*18.1416*	*11.5*	*0.6220*	*12.9*	*0.0818*	*5.8*	*0.45*	*507.1*	*28.5*	*491.1*	*50.3*	*417.2*	*257.6*	*507.1*	*28.5*	*NA*
90	2.0	2.0	102071	6.0162	2.6	8.5508	6.7	0.3731	6.2	0.92	2044.0	108.6	2291.3	61.1	2519.9	43.1	2519.9	43.1	81.1
91	2.7	1.3	57563	16.9533	6.2	0.6533	9.0	0.0803	6.6	0.73	498.0	31.4	510.5	36.3	566.6	135.4	498.0	31.4	87.9
92	304	1.9	44262	16.5215	6.5	0.6743	8.2	0.0808	5.1	0.62	500.9	24.6	523.3	33.7	622.5	139.7	500.9	24.6	80.5
93	75	1.3	67280	10.4553	5.3	3.2374	8.1	0.2455	6.1	0.76	1415.2	77.8	1466.2	62.7	1540.8	99.1	1540.8	99.1	91.8
94	330	1.3	36368	17.0036	4.4	0.6574	5.2	0.0811	2.8	0.54	502.5	13.5	513.0	21.0	560.1	96.0	502.5	13.5	89.7
95	*174*	*1.6*	*33358*	*18.6043*	*19.5*	*0.6167*	*20.0*	*0.0832*	*4.3*	*0.21*	*515.2*	*21.1*	*487.8*	*77.5*	*360.6*	*443.7*	*515.2*	*21.1*	*NA*
96	*187*	*2.1*	*27950*	*17.4138*	*9.9*	*0.6215*	*13.2*	*0.0785*	*8.7*	*0.66*	*487.1*	*40.7*	*490.8*	*51.3*	*507.9*	*218.2*	*487.1*	*40.7*	*NA*
97	449	1.5	81510	13.7030	2.3	1.6741	3.9	0.1664	3.2	0.81	992.1	29.0	998.8	24.8	1013.3	46.6	1013.3	46.6	97.9
98	499	1.1	79240	16.8682	2.4	0.8002	4.0	0.0979	3.2	0.80	602.1	18.7	596.9	18.2	577.5	52.3	602.1	18.7	104.3
99	*149*	*1.1*	*31720*	*20.4058*	*18.7*	*0.5584*	*21.9*	*0.0826*	*11.5*	*0.52*	*511.8*	*56.6*	*450.5*	*80.0*	*148.1*	*441.3*	*511.8*	*56.6*	*NA*
100	212	1.6	25701	16.4020	9.0	0.8228	10.3	0.0979	5.0	0.49	602.0	28.7	609.6	47.1	638.1	193.4	602.0	28.7	94.3
Sample: VFNO49																			
1	26	7.5	6686	11.8521	14.6	1.9734	29.4	0.1696	25.5	0.87	1010.1	238.6	1106.5	200.5	1301.2	284.5	1301.2	284.5	77.6
2	299	2.5	109210	13.6267	3.9	1.6120	5.0	0.1593	3.2	0.63	953.0	28.0	974.9	31.4	1024.6	78.8	1024.6	78.8	93.0
3	300	1.1	50050	15.6624	3.0	1.0972	5.7	0.1246	4.8	0.85	757.2	34.6	752.0	30.4	736.6	64.5	757.2	34.6	102.8
4	304	1.1	49614	17.2639	7.6	0.6971	9.2	0.0873	5.1	0.56	539.5	26.6	537.1	38.2	526.9	166.6	539.5	26.6	102.4
5	461	4.1	107304	16.9413	3.1	0.8405	3.7	0.1033	2.1	0.56	633.5	12.6	619.4	17.2	568.1	66.8	633.5	12.6	111.5
6	256	3.0	887	11.6946	12.1	1.4232	12.3	0.1207	1.9	0.16	734.7	13.5	898.7	73.3	1327.1	235.3	1327.1	235.3	55.4
7	153	1.8	97502	11.8505	5.4	2.6445	6.7	0.2273	3.9	0.59	1320.3	47.0	1313.1	49.4	1301.4	105.5	1301.4	105.5	101.5
8	159	0.6	18837	17.4503	15.5	0.6765	16.1	0.0856	4.3	0.27	529.6	21.9	524.7	66.2	503.3	344.1	529.6	21.9	105.2
10	237	1.6	37023	17.3350	6.0	0.6491	7.1	0.0816	3.8	0.54	505.7	18.6	507.9	28.4	517.9	131.6	505.7	18.6	97.7
11	567	3.0	136986	13.4472	1.1	1.7406	4.3	0.1698	4.2	0.96	1010.8	38.9	1023.7	27.8	1051.4	23.2	1051.4	23.2	96.1
12	200	1.7	40394	13.1869	2.2	1.8316	4.0	0.1752	3.3	0.84	1040.6	31.8	1056.9	26.0	1090.6	43.7	1090.6	43.7	95.4
13	231	1.6	24595	13.8807	7.1	1.6596	8.5	0.1671	4.7	0.55	996.0	43.1	993.2	53.7	987.2	143.8	987.2	143.8	100.9
14	262	2.6	71952	14.9978	2.8	1.2103	4.5	0.1317	3.6	0.79	797.3	26.7	805.3	25.2	827.7	58.4	797.3	26.7	96.3
15	215	1.3	28627	16.7120	8.3	0.7340	10.5	0.0890	6.4	0.61	549.4	33.5	558.9	45.0	597.7	180.1	549.4	33.5	91.9
16	348	2.6	63552	16.9961	7.8	0.6596	9.4	0.0813	5.3	0.57	503.9	25.9	514.4	38.1	561.1	170.0	503.9	25.9	89.8
17	222	0.9	61270	13.9834	4.9	1.4742	6.4	0.1495	4.2	0.65	898.2	34.9	919.8	38.8	972.1	99.7	972.1	99.7	92.4
18	180	1.2	34018	17.9656	18.8	0.6765	20.4	0.0881	7.8	0.38	544.6	40.9	524.7	83.7	438.9	421.9	544.6	40.9	NA

19	464	1.3	66788	16.2616	2.6	0.8599	6.6	0.1014	6.1	0.92	622.7	36.3	630.1	31.2	656.6	55.4	622.7	36.3	94.8
20	233	9.5	29964	17.9644	11.3	0.5859	13.5	0.0763	7.5	0.55	474.3	34.3	468.3	50.9	439.0	251.8	474.3	34.3	NA
21	459	0.5	69646	16.3034	3.2	0.8754	5.8	0.1035	4.9	0.84	635.0	29.6	638.5	27.6	651.1	67.7	635.0	29.6	97.5
22	508	0.9	135208	9.3904	0.8	3.7994	3.5	0.2588	3.4	0.97	1483.5	45.4	1592.6	28.4	1740.2	15.3	1740.2	15.3	85.2
23	186	2.2	26648	17.7640	15.3	0.6519	15.8	0.0840	3.7	0.23	519.9	18.3	509.6	63.3	463.9	341.7	519.9	18.3	NA
24	364	1.0	67184	17.0094	4.3	0.6750	4.7	0.0833	1.8	0.39	515.6	9.0	523.7	19.1	559.4	93.8	515.6	9.0	92.2
25	105	0.7	44110	12.9457	7.3	1.7006	9.4	0.1597	5.8	0.62	954.9	51.4	1008.8	59.9	1127.5	146.6	1127.5	146.6	84.7
26	662	2.2	94068	16.3171	3.3	0.8835	4.3	0.1045	2.8	0.65	641.0	17.3	642.8	20.7	649.3	70.6	641.0	17.3	98.7
27	720	4.7	196223	13.5933	1.9	1.7203	4.9	0.1696	4.5	0.92	1009.9	42.1	1016.1	31.4	1029.6	38.5	1029.6	38.5	98.1
28	295	1.2	42727	17.9327	6.3	0.6702	7.4	0.0872	3.8	0.52	538.8	19.9	520.8	30.2	443.0	141.2	538.8	19.9	NA
29	130	5.1	27825	14.1124	9.1	1.6684	10.5	0.1708	5.4	0.51	1016.3	50.5	996.6	67.0	953.4	186.1	953.4	186.1	106.6
30	343	1.2	74412	17.1957	7.4	0.6872	8.7	0.0857	4.6	0.52	530.1	23.3	531.1	36.2	535.6	163.2	530.1	23.3	99.0
31	212	1.5	29606	18.0132	6.9	0.6127	8.1	0.0800	4.4	0.53	496.4	20.8	485.3	31.4	433.0	153.6	496.4	20.8	NA
33	206	2.2	46851	13.8912	5.9	1.5493	8.5	0.1561	6.1	0.72	935.0	53.2	950.2	52.6	985.6	120.9	985.6	120.9	94.9
34	226	1.9	73018	13.3241	2.2	1.6928	6.8	0.1636	6.5	0.95	976.6	58.8	1005.8	43.7	1069.9	43.6	1069.9	43.6	91.3
35	367	1.2	130485	11.9062	2.2	2.6123	3.5	0.2256	2.7	0.78	1311.3	32.4	1304.1	25.6	1292.3	42.0	1292.3	42.0	101.5
36	168	9.0	41866	17.6779	15.2	0.6595	16.0	0.0846	5.1	0.32	523.3	25.7	514.3	64.7	474.7	337.4	523.3	25.7	NA
37	507	0.9	105093	15.9398	3.4	0.9870	4.2	0.1141	2.4	0.57	696.5	15.7	697.2	21.1	699.3	73.3	696.5	15.7	99.6
38	133	1.6	9770	16.8063	13.2	0.7003	15.0	0.0854	7.2	0.48	528.0	36.3	539.0	62.8	585.5	287.0	528.0	36.3	90.2
39	309	5.8	46445	18.1938	5.9	0.5813	11.1	0.0767	9.4	0.85	476.4	43.1	465.3	41.3	410.7	131.2	476.4	43.1	NA
40	40	2.7	27462	7.2762	4.9	7.4613	6.4	0.3937	4.0	0.63	2140.2	73.7	2168.3	57.1	2195.1	85.7	2195.1	85.7	97.5
41	644	3.0	123373	15.8263	2.9	0.9829	4.5	0.1128	3.5	0.77	689.1	22.6	695.1	22.7	714.5	61.6	689.1	22.6	96.4
42	368	2.6	47430	16.9248	4.3	0.7055	11.2	0.0866	10.3	0.92	535.4	53.1	542.1	47.0	570.3	92.8	535.4	53.1	93.9
43	583	4.4	103019	14.1159	2.2	1.4175	5.2	0.1451	4.7	0.91	873.6	38.4	896.3	30.9	952.9	45.0	952.9	45.0	91.7
44	425	3.0	711450	5.9273	0.8	8.9689	3.4	0.3856	3.3	0.97	2102.2	59.8	2334.8	31.4	2544.9	13.7	2544.9	13.7	82.6
45	307	1.5	39553	17.2715	5.7	0.6587	6.6	0.0825	3.3	0.50	511.1	16.2	513.8	26.5	525.9	124.4	511.1	16.2	97.2
46	699	4.6	93990	13.1993	1.3	1.9676	11.9	0.1884	11.8	0.99	1112.5	120.5	1104.5	80.0	1088.8	26.2	1088.8	26.2	102.2
47	217	2.0	39565	15.7696	7.8	0.7630	9.7	0.0873	5.8	0.60	539.4	29.8	575.7	42.5	722.1	164.7	539.4	29.8	74.7
48	117	1.5	32252	17.6372	14.4	0.9071	15.6	0.1160	6.0	0.39	707.7	40.5	655.5	75.5	479.8	319.2	707.7	40.5	147.5
49	122	1.8	18246	18.3871	20.9	0.6417	22.1	0.0856	7.1	0.32	529.3	35.9	503.4	87.9	387.0	474.6	529.3	35.9	NA
50	163	1.6	22013	16.3916	13.6	0.7454	14.4	0.0886	4.7	0.32	547.3	24.5	565.5	62.6	639.5	294.5	547.3	24.5	85.6
51	100	1.4	28675	17.4422	22.7	0.6924	25.0	0.0876	10.7	0.43	541.3	55.4	534.3	104.4	504.4	504.5	541.3	55.4	107.3
52	130	1.3	12326	18.1202	18.0	0.6082	21.1	0.0799	11.1	0.52	495.7	52.8	482.4	81.4	419.8	405.4	495.7	52.8	NA
53	353	2.2	60207	17.5692	5.1	0.6210	6.2	0.0791	3.5	0.56	490.9	16.4	490.5	24.1	488.3	113.5	490.9	16.4	NA
55	381	1.6	100032	16.8762	3.0	0.8390	3.9	0.1027	2.4	0.62	630.2	14.6	618.6	18.1	576.5	66.3	630.2	14.6	109.3
56	291	5.3	107272	16.6376	6.7	0.7592	8.7	0.0916	5.6	0.64	565.0	30.1	573.5	38.3	607.3	146.0	565.0	30.1	93.0
57	692	13.0	156290	13.6541	1.7	1.6119	4.0	0.1596	3.7	0.91	954.7	32.6	974.8	25.4	1020.5	34.3	1020.5	34.3	93.5
58	52	1.2	12434	13.5869	13.1	1.7916	13.7	0.1765	4.1	0.30	1048.1	39.4	1042.4	89.5	1030.5	265.5	1030.5	265.5	101.7
59	335	0.8	43070	16.3383	3.6	0.9506	4.3	0.1126	2.3	0.55	688.1	15.2	678.4	21.0	646.5	76.5	688.1	15.2	106.4
60	177	1.1	56901	9.4812	11.1	4.2975	11.8	0.2955	4.1	0.35	1669.0	60.4	1692.9	97.7	1722.5	204.3	1722.5	204.3	96.9
62	359	2.2	161311	13.4000	1.7	1.8947	2.5	0.1841	1.9	0.74	1089.6	18.8	1079.2	16.8	1058.5	34.0	1058.5	34.0	102.9
63	208	1.9	65871	14.9773	3.6	1.1542	5.2	0.1254	3.7	0.71	761.4	26.3	779.2	28.1	830.5	75.7	761.4	26.3	91.7
64	410	5.1	126567	16.7198	4.3	0.7377	8.7	0.0895	7.5	0.87	552.3	39.8	561.0	37.4	596.7	94.0	552.3	39.8	92.6
65	324	0.8	63939	17.1491	8.1	0.6698	8.7	0.0833	3.1	0.35	515.8	15.2	520.6	35.3	541.5	177.3	515.8	15.2	95.3
66	142	1.6	33747	13.9584	7.7	1.5651	10.2	0.1584	6.6	0.65	948.1	58.1	956.5	63.1	975.8	157.9	975.8	157.9	97.2
67	253	1.2	92228	13.2135	3.9	1.7274	7.2	0.1655	6.1	0.84	987.5	55.5	1018.8	46.6	1086.6	79.1	1086.6	79.1	90.9
68	635	3.5	160403	16.4187	2.8	0.8741	4.2	0.1041	3.2	0.75	638.3	19.3	637.8	20.1	635.9	60.2	638.3	19.3	100.4
69	450	6.8	89994	16.3860	5.7	0.8798	7.5	0.1046	4.8	0.65	641.0	29.5	640.9	35.5	640.2	122.2	641.0	29.5	100.1
70	378	1.3	85354	16.5282	4.0	0.8472	6.1	0.1016	4.5	0.75	623.6	26.9	623.1	28.2	621.6	86.5	623.6	26.9	100.3
71	389	7.0	31452	16.5121	3.8	0.8767	4.3	0.1050	2.0	0.47	643.6	12.3	639.2	20.4	623.7	82.1	643.6	12.3	103.2
72	189	2.6	39752	14.3277	7.9	1.4720	8.6	0.1530	3.4	0.40	917.5	29.5	918.9	52.3	922.3	163.3	922.3	163.3	99.5
73	84	2.4	22633	11.3090	4.2	2.8428	5.4	0.2332	3.5	0.64	1351.1	42.4	1366.9	40.8	1391.7	79.9	1391.7	79.9	97.1
74	401	2.0	14101	16.1953	7.4	0.7755	8.2	0.0911	3.6	0.44	562.0	19.3	582.9	36.4	665.4	158.2	562.0	19.3	84.5
75	381	1.1	44774	17.3013	4.0	0.6301	4.8	0.0791	2.6	0.55	490.5	12.4	496.1	18.9	522.1	88.7	490.5	12.4	93.9
76	138	1.0	19608	16.9395	14.0	0.7310	14.8	0.0898	4.8	0.32	554.4	25.5	557.2	63.6	568.4	306.5	554.4	25.5	97.5
77	298	0.8	36269	15.8990	6.9	0.8128	9.0	0.0937	5.7	0.64	577.5	31.7	604.0	41.0	704.7	147.8	577.5	31.7	81.9
78	111	2.0	94125	3.6978	0.8	25.5005	2.3	0.6839	2.1	0.93	3359.3	56.2	3327.6	22.5	3308.5	13.1	3308.5	13.1	101.5
79	539	1.4	84002	16.2983	2.9	0.9240	7.0	0.1092	6.3	0.91	668.2	40.0	664.5	33.9	651.8	63.3	668.2	40.0	102.5
80	325	2.3	236417	10.6994	1.6	3.4148	2.4	0.2650	1.8	0.76	1515.3	24.8	1507.8	19.0	1497.3	29.9	1497.3	29.9	101.2

(*continued on next page*)

Table 2 (*continued*)

	Isotopic ratios										Apparent ages (Ma)								
	U, ppm	U/Th	$^{206}Pb^*/^{204}Pb$	$^{206}Pb^*/^{207}Pb^*$	±(%)	$^{207}Pb^*/^{235}U^*$	±(%)	$^{206}Pb^*/^{238}U$	±(%)	Error Corr.	$^{206}Pb^*/^{238}U^*$	±(Ma)	$^{207}Pb^*/^{235}U$	±(Ma)	$^{206}Pb^*/^{207}Pb^*$	±(Ma)	Best age (Ma)	(Ma)	Conc. (%)
81	133	1.4	12824	15.9215	14.9	0.8457	15.4	0.0977	3.8	0.25	600.6	21.9	622.3	71.6	701.8	318.7	600.6	21.9	85.6
82	392	1.0	63117	15.5262	4.9	0.9244	6.4	0.1041	4.1	0.65	638.3	25.1	664.7	31.2	755.0	103.0	638.3	25.1	84.5
83	205	2.3	108717	13.5288	3.3	1.6793	4.8	0.1648	3.4	0.72	983.2	31.5	1000.7	30.6	1039.2	67.5	1039.2	67.5	94.6
84	268	1.6	41554	14.5295	6.6	1.1597	19.8	0.1222	18.7	0.94	743.3	131.3	781.8	108.5	893.5	135.9	743.3	131.3	83.2
85	151	2.8	77254	13.3504	5.7	1.3838	6.3	0.1340	2.7	0.43	810.6	20.6	882.1	37.4	1065.9	115.3	1065.9	115.3	76.0
86	173	2.1	48586	13.6723	4.0	1.7411	5.5	0.1726	3.7	0.68	1026.7	35.5	1023.9	35.3	1017.8	81.0	1017.8	81.0	100.9
87	86	1.7	37317	14.1227	7.4	1.6277	10.3	0.1667	7.2	0.70	994.0	66.4	981.0	65.0	951.9	151.5	951.9	151.5	104.4
90	566	2.6	135462	15.2535	3.3	1.1958	4.0	0.1323	2.3	0.56	800.9	17.1	798.7	22.3	792.3	69.8	800.9	17.1	101.1
91	248	2.4	76190	17.2841	12.7	0.7123	13.7	0.0893	5.2	0.38	551.3	27.3	546.1	58.0	524.3	279.8	551.3	27.3	105.2
92	155	1.1	73610	9.4887	1.5	4.6026	2.5	0.3167	2.0	0.79	1773.8	30.6	1749.7	20.8	1721.1	27.9	1721.1	27.9	103.1
93	263	1.0	47706	17.3244	8.1	0.6918	10.3	0.0869	6.3	0.62	537.3	32.7	533.9	42.8	519.2	178.5	537.3	32.7	103.5
94	161	0.5	21576	17.8378	11.1	0.6879	12.4	0.0890	5.5	0.44	549.6	28.8	531.6	51.3	454.8	247.3	549.6	28.8	120.9
95	93	1.3	30551	13.1873	11.3	1.6324	13.1	0.1561	6.6	0.50	935.2	57.4	982.8	82.5	1090.6	226.7	1090.6	226.7	85.8
96	405	0.6	269553	8.9149	1.4	4.8300	2.8	0.3123	2.5	0.88	1752.0	38.1	1790.1	23.8	1834.9	24.6	1834.9	24.6	95.5
97	330	1.5	31183	16.9955	6.3	0.6522	6.7	0.0804	2.4	0.36	498.4	11.6	509.8	27.0	561.2	137.3	498.4	11.6	88.8
98	179	2.4	23914	17.7551	9.4	0.8451	9.8	0.1088	2.8	0.29	665.9	17.8	622.0	45.8	465.1	209.5	665.9	17.8	143.2
99	172	2.0	36275	16.7740	20.8	0.6654	21.4	0.0809	4.8	0.22	501.8	23.1	517.9	87.0	589.7	456.7	501.8	23.1	85.1
100	316	2.7	55544	18.2562	8.2	0.6556	9.1	0.0868	4.0	0.44	536.6	20.4	511.9	36.6	403.1	183.4	536.6	20.4	NA

All uncertainties are reported at the 1-sigma level, and include only measurement errors. Systematic errors would increase the uncertainty of clusters of ages by 1–2%.
U concentration and U/Th are calibrated relative to a Sri Lanka zircon and are accurate to ~20% Pb correction.
U/Pb and $^{206}Pb/^{207}Pb$ fractionation is calibrated relative to fragments of a large Sri Lanka zircon of 564 Ma age (2-sigma).
U decay constants and composition as follows: $^{238}U = 9.8485 \times 10^{-10}$, $^{235}U = 1.55125 \times 10^{-10}$, $^{238}U/^{235}U = 137.88$.
Best age is determined from $^{206}Pb/^{238}U$ age for analyses with $^{206}Pb/^{238}U$ age <900 Ma and from $^{206}Pb/^{207}Pb$ age for analyses with $^{206}Pb/^{238}U$ age > 900 Ma.
Concordance is based on $^{206}Pb/^{238}U$ age/$^{206}Pb/^{207}Pb$ age. NA denotes that value is not reported for $^{206}Pb/^{238}U$ ages < 500 Ma because of large uncertainty in $^{206}Pb/^{207}Pb$ age.
Analyses with $^{206}Pb/^{238}U$ age > 500 Ma and with >30% discordance (<70% concordance) are not included, and remarked with italics.
Analyses with $^{206}Pb/^{238}U$ age > 500 Ma and with >5% reverse discordance (<105% concordance) are not included.

northern tip of the Sierra de Valle Fértil, near the southernmost outcrop of the Early Ordovician batholith (Figs. 1and 2). Hence, sample VFSCH22 provides information about the provenance of sedimentary successions exposing the inferred deepest exposed levels of the Early Ordovician arc (Otamendi et al., 2008), whereas samples VFNO49 and VFNO28 come from sedimentary sequences buried to mid-crustal paleodepths at the inferred root of the Famatina batholith. Moreover, the close proximity of the latter two samples to the Sierra de Famatina allows for direct comparison with the early Paleozoic sedimentary succession that appears as screens or roof of the batholith at upper crustal levels (e.g., Collo et al., 2009).

Metasedimentary rocks in the Sierra de Valle Fértil were metamorphosed at granulite–facies temperatures during Early Ordovician magmatism. Despite this high grade of metamorphism, in most outcrops the protoliths for these rocks can be recognized as a turbiditic sand/silt/shale succession.

Stromatic migmatite VFSCH22 comes from a large metasedimentary septum enclosed by gabbroic and dioritic rocks from the mafic unit (Otamendi et al., 2009), located approximately 20 km WSW of Las Juntas in the western Sierra de Valle Fértil (Fig. 2). The metamorphic assemblage is quartz + plagioclase + biotite + sillimanite + garnet ± cordierite ± K-feldspar, characteristic of granulite–facies equivalent conditions (Fig. 3A). The best estimates of peak metamorphic conditions are temperatures of 800–820 °C and pressures of ~8 kbar (unpublished data). At the microscopic scale, clusters of biotite flakes are associated with long prismatic sillimanite wrapping around or cutting across garnet porphyroblasts. Kinked twins and dynamic recrystallization of feldspar are associated with protomylonitic fabrics (Fig. 3B).

Paragneissic migmatites VFNO28 and VFNO49 are from the northern part of the Sierra de Valle Fértil, located ~5 km SE of Ischigualasto National Park. In this area, metasedimentary packages attained granulite–facies temperatures, although compositional layering of meta-graywackes and metapelites is likely relict bedding of a turbiditic succession. The metamorphic assemblage for metasedimentary rocks in the northern Sierra de Valle Fértil is quartz + plagioclase + biotite + cordierite ± garnet ± sillimanite ± K-feldspar (Fig. 3C and D), and allows us to estimate that they attained granulite–facies temperatures (800 ± 40 °C at pressures of approximately 6.0–6.5 kbar (Tibaldi et al., 2011). Most quartz grains exhibit extensive development of internal sub-grains reflecting weak strain after peak temperature conditions.

4. U–Pb detrital zircon geochronology

4.1. Methodology

Zircon separation was performed at Universidad Nacional de Río Cuarto in Argentina following conventional magnetic and heavy liquid techniques. We analyzed three detrital samples from the Sierra de Valle Fértil (Table 1; Fig. 2). U–Pb geochronologic analyses were conducted on individual zircon grains. Zircons were analyzed by laser-ablation multicollector inductively-coupled plasma mass spectrometry (LA-MC-ICPMS) using a Nu Plasma HR MC-ICPMS at the University of Arizona. All analyses were conducted using a spot diameter of 25 microns. Inter-element fractionation of Pb/U was generally ~5%, whereas apparent fractionation of Pb isotopes was generally <0.2%. In-run analysis of fragments of a large zircon crystal with a known age of 563.5 ± 3.2 Ma (2σ error) was used to correct for this fractionation. The uncertainty resulting from the calibration correction is generally 1–2% (2σ) for both $^{206}Pb/^{207}Pb$ and $^{206}Pb/^{238}U$ ages. Concentrations of U and Th were calibrated relative to a Sri Lanka zircon standard. In Table 2 asterisks denotes common Pb corrections. Analytical results are reported in Table 2. Uncertainties shown in this table are at the 1σ level, and include only measurement errors. Further details about equipment, analytical procedures and sources of error are given in Gehrels et al. (2008).

Random populations of 100 grains were dated from each sample. However, to minimize the inclusion of age data that are not representative of detrital age populations, we excluded analyses that meet any of the following criteria: 1) >30% discordant (<70% concordance by comparison of $^{206}Pb/^{238}U$ and $^{206}Pb/^{207}Pb$ ages), 2) >5% reverse discordant (<105% concordance), or 3) $^{206}Pb/^{238}U$ ages <500 Ma with large uncertainties. These excluded data are reported in italics in Table 2. The consistency of the filtered data subset was then tested by projecting on concordia plots (Fig. 4) that are constructed using the routines in Isoplot (Ludwig, 2003). DZ age spectra are shown on combined probability density and histogram diagrams (Fig. 5). Due to the increasing uncertainty of $^{206}Pb/^{238}U$ ages and the decreasing uncertainty of $^{206}Pb/^{207}Pb$ ages as a function of age, we used $^{206}Pb^*/^{238}U$ ages for <900 Ma grains and $^{206}Pb^*/^{207}Pb^*$ for >900 Ma grains.

To compare DZ provenance at a regional scale, detrital zircon age spectra are shown on relative age-probability diagrams (Fig. 6). These composite age probability plots normalize each curve according to the number of constituent analyses, such that each curve contains the same area, and then stacks the probability curves (Gehrels et al., 2008). As shown in Fig. 6, the combination of several DZ spectra better fingerprint sources than any single spectrum (Gehrels et al., 2000).

Maximum depositional ages (MDA) estimated from U–Pb DZ geochronology provide valuable information for correlating tectonostratigraphic units at regional scales. The youngest age cluster in a sample defined by three or more overlapping (2σ) analyses provides the most reliable MDA (e.g., Dickinson and Gehrels, 2009). Although, quartz-rich siliciclastic layers tend to be refractory and do not undergo partial melting during granulite–facies metamorphism, the high grade metamorphic history of these rocks complicates our ability to extract detailed age information from individual analyses.

4.2. Results

Overall, the three samples display polymodal and similar DZ age patterns, with three main age populations corresponding to Early and Middle Cambrian, late Neoproterozoic and Mesoproterozoic time (Fig. 5; geological timescale of Ogg et al., 2008). The peaks at ~520 Ma and ~1050 Ma are the most dominant; the late Neoproterozoic DZ cluster varies between 580 and 640 Ma. Another notable aspect of Valle Fértil metasedimentary DZ patterns is the presence of Paleo-proterozoic (1.9–2.2 Ma) and Neoarchean (2.5–2.6 Ga) age peaks in all the specimens. The age spectra of DZ samples are consistent with derivation from magmatic and recycled sediments involved in the Pampean orogeny (Adams et al., 2008).

Specimen VFSCH22 collected at the western boundary of the Sierra de Valle Fértil is different from the other two samples (VFNO28 and VFNO49) in that it has relatively fewer Cambrian and more Mesoproterozoic ages. This sample yielded five $^{206}Pb/^{238}U$ individual zircon ages that vary from 460 to 489 Ma. These relatively young ages are interpreted to reflect metamorphic zircon growth, because they closely overlap with the full range of magmatic zircon ages in the same crustal section (e.g., Ducea et al., 2010). Excluding these younger metamorphic zircons, a dominant population of inherited ages supports the conservative conclusion that the sedimentary protolith to this migmatite was deposited after the Middle Cambrian.

Sample VFNO28 includes less metamorphic grains and contains a significant cluster of grains that yield an MDA of 512 ± 16 Ma (2σ error). Notably, an almost identical MDA of 518 ± 12 Ma is estimated for sample VFNO49, using a coherent population pooled

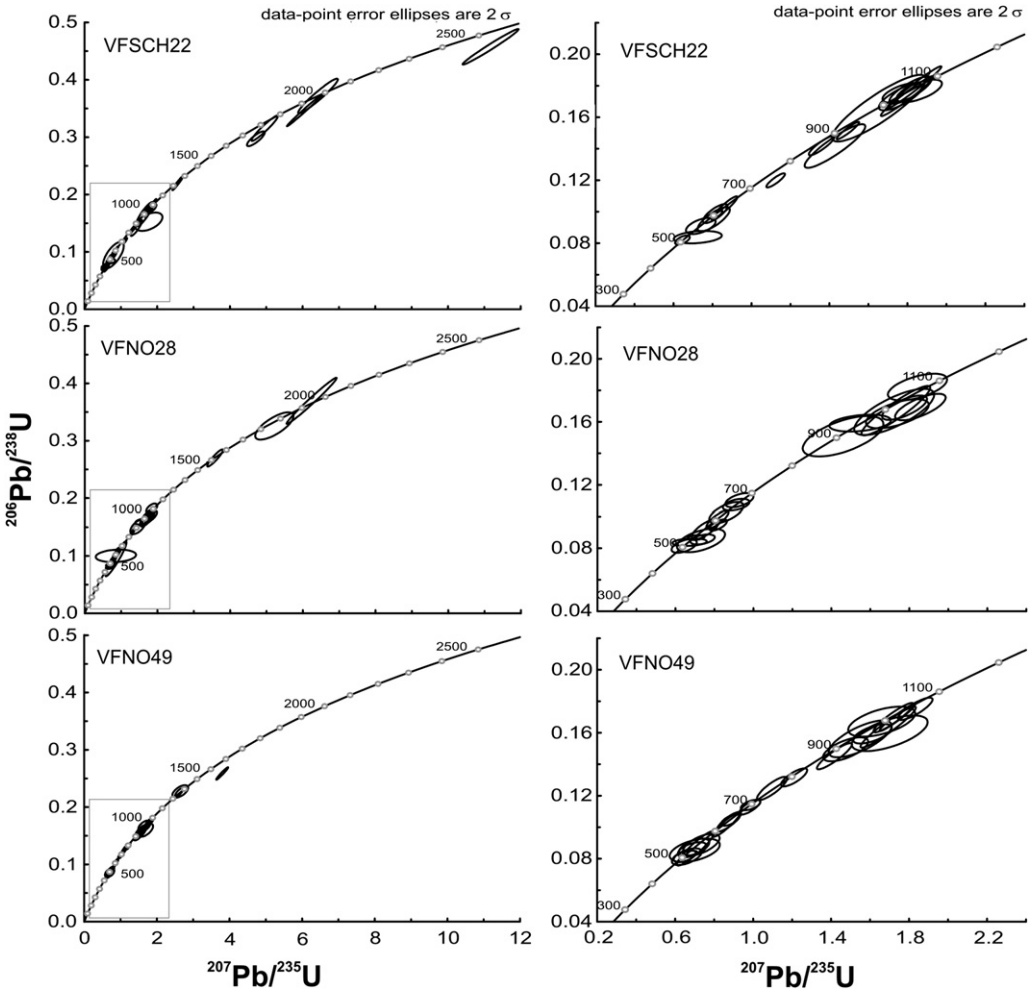

Fig. 4. Conventional concordia diagrams for LAM-MC-ICP-MS analyses of zircons for metasedimentary samples from the Sierra de Valle Fértil, constructed with Isoplot (Ludwig, 2003). Relative errors are shown as ellipses at the 2σ levels. On the right side the concordia plots exclude older analyses, illustrating that age clusters are robust and restricted.

from the six youngest ages. These two rocks yield MDA that fall in the range of maximum depositional ages estimated for the Mesón Group (e.g., Adams et al., 2010).

5. Discussion

5.1. Provenance and age of metasedimentary rock in the Sierra de Valle Fértil

The prominent peaks of constituent age populations at 520 Ma, 600 Ma, and 1050 Ma reflect derivation from early Paleozoic, late Neoproterozoic, and Grenvillian sources near the West Gondwanan margin (Fig. 6). Most of the zircons from the youngest dominant age peak (ca. 520 Ma) were likely eroded from the active Lower Cambrian Pampean arc.

At a finer level of detail, the youngest coherent cluster of DZ ages in the Sierra de Valle Fértil metasediments of about 518 Ma reveals that the sedimentary precursors were deposited during Middle Cambrian time or even younger. This relatively young depositional age is supported by the similarity of DZ age spectra for the Sierra de Valle Fértil metasedimentary rocks to those of Negro Peinado and Achavil Formation of the Sierra de Famatina and Mesón Group in the Cordillera Oriental and Puna (Fig. 6). The existence of a Lower Cambrian DZ age peak is a distinctive feature characterizing Middle to Upper Cambrian sedimentary successions as compared with the latest Neoproterozoic to Lower Cambrian sequences, given that Pampean magmatism did not initiate until about 540 Ma and only began supplying young zircons after its inception (Adams et al., 2008, 2010; Collo et al., 2009).

In northwestern Argentina, Cambrian strata correlate to a regional scale tectonic boundary called the Tilcaric orogeny (Turner, 1960). The Tilcaric deformation event, which resulted in deformed and uplifted Puncoviscana Formation, predates the deposition of Middle and Upper Cambrian successions (Turner, 1960; Aceñolaza and Miller, 1982; Durand, 1996). In regions of intense Ordovician deformation, recognition of the structural features and/or the tectonic unconformity that typifies the Tilcaric event is difficult or impossible. DZ studies thereby provide the strongest criteria for correlating metasedimentary rocks (Piñán-Llamas and Simpson, 2006). Following previous arguments, we suggest that the age of deposition and the source for the detritus in the Sierra de Valle Fértil metasedimentary rocks are the same as those proposed for sedimentary successions of similar age in the Sierras de Famatina, Cordillera Oriental and Puna.

The existence of well-defined Grenvillian DZ age peaks implies regional sources with exposed Mesoproterozoic crystalline rocks supplying zircons and/or recycling of older Puncoviscana sedimentary successions (e.g., Adams et al., 2008; 2010). The nearest potential source of Grenvillian detritus to the early Paleozoic basins considered here was likely the Sunsás province in northwestern Argentina and Bolivia (Chew et al., 2007). However, Mesoproterozoic and late Neoproterozoic DZ age populations from Middle to

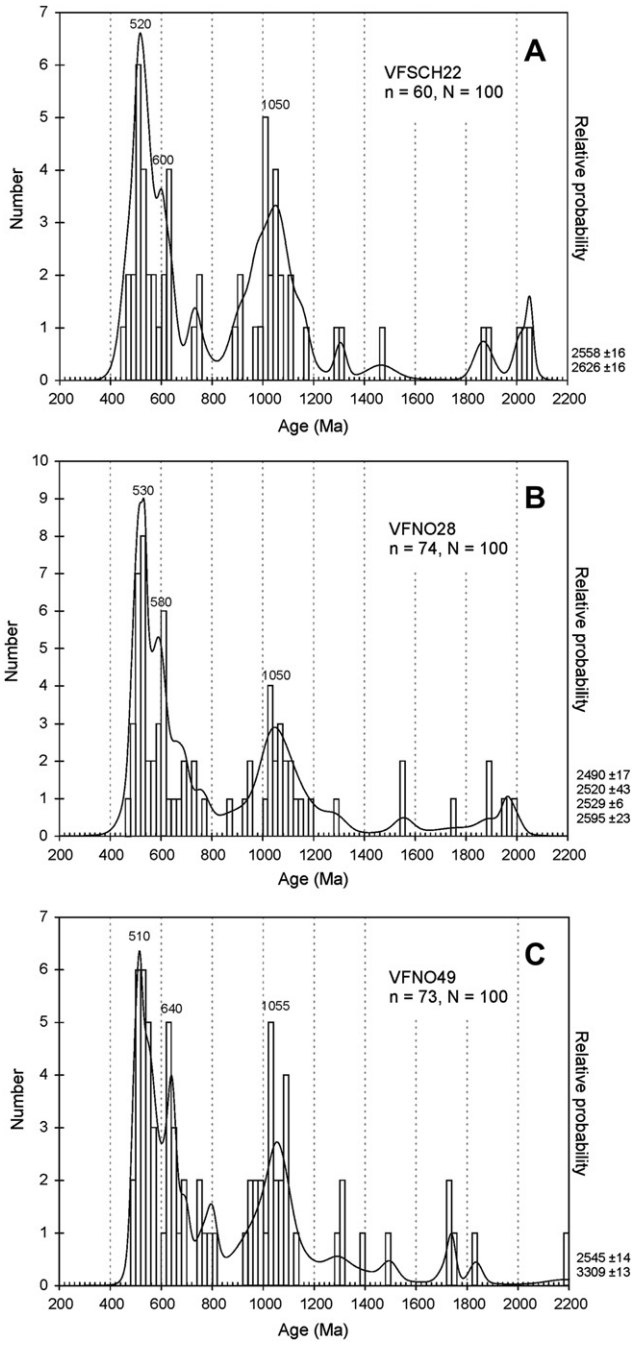

Fig. 5. Combined histograms overlain by true probability plots, illustrating the detrital zircon age spectrum for metasediments from Valle Fértil. The number of analyses (*y*-axis) gives the number of ages which fall in each histogram bin. Along the *x*-axis each plot covers a range in ages from 200 to 2200 Ma with 20 Ma bin widths. Ages < 900 Ma are $^{206}Pb/^{238}U$ analyses, ages > 900 Ma are $^{207}Pb/^{206}Pb$ analyses. Ages older than 2200 Ma are listed at the right margin.

Late Cambrian sedimentary successions closely resemble those of nearby Puncoviscana Formation, and recycling from these rocks is perhaps more reasonable than the option that long rivers carried detritus from a cratonic area complexly composed of Grenvillian and Brasiliano–Pan-African crystalline rocks (Fig. 1). From a somewhat different perspective, Collo et al. (2009) drew the same conclusion, as they showed that the immature textural and mineralogical nature of Middle and Upper Cambrian sandstones of the Famatina reflect derivation from the Pampean orogen forming nearby. Recent studies showed that the Sunsás orogen extended further to the south than previously thought (Gaucher et al., 2010; Chernicoff et al., 2012), possibly contributing detritus to late Cambrian depocenters now preserved along central–northwestern Argentina.

In southern South America, Neoproterozoic zircon populations are thought to be derived from Brasiliano–Pan-Africa orogens that formed during the amalgamation of West Gondwana (de Brito Neves and Cordani, 1991). This was a collection of continental-scale collisional orogens, which together resemble the present-day Mediterranean-Himalayan orogenic belts (Trompette, 1997). The extent of magmatism and metamorphism along Brasiliano–Pan-African orogenesis in the absence of coeval large-scale orogenies in Laurentia has been considered to be the diagnostic feature demonstrating DZ inheritance from Gondwanan sources (Schwartz and

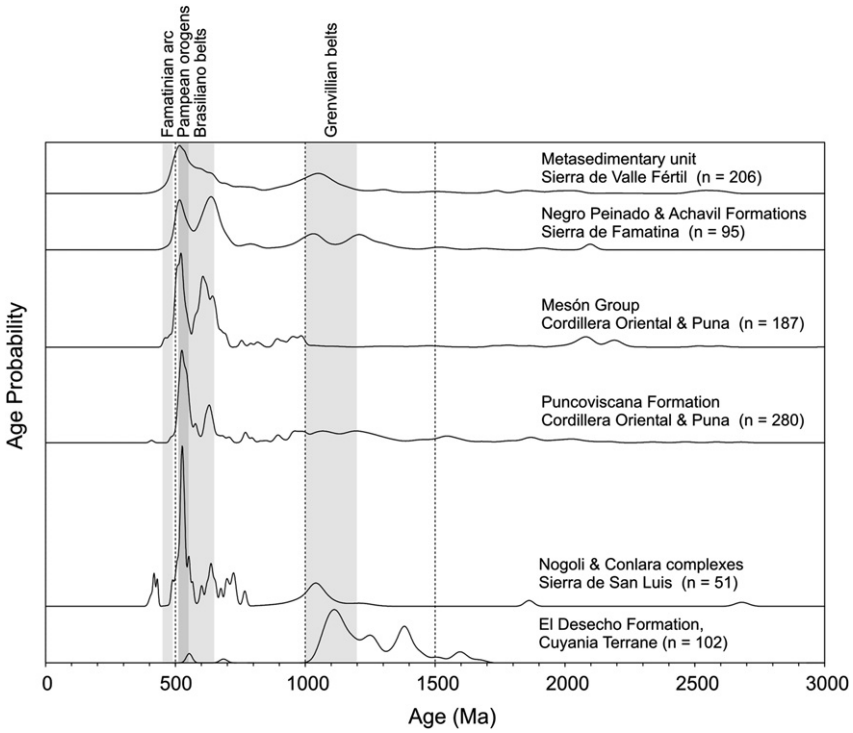

Fig. 6. U–Pb detrital zircon age spectra that compare Sierra de Valle Fértil metasediments with other sedimentary successions with similar depositional ages of central and northwestern Argentina. Detrital zircon ages are compiled from: Collo et al. (2009) for Negro Peinado and Achavil Formations, Adams et al. (2010) for Mesón Group and Puncoviscana Formations, Drobe et al. (2009) for Pringles and Nogoli metamorphic complexes, and Naipauer et al. (2010) for El Desecho Formation. The number (*n*) in each plot gives the total number grains utilized to obtain a composite from each tectonostratigraphic zone; however, the total area below each pattern is independent of this number. Refer to Fig. 7 for locations of each of the tectonostratigraphic units. The time span of the orogenic systems from southern South America, which is shown as vertical gray bars, is taken from the literature presented in the text. The plot was constructed with the excel file named normalized probability plot as updated at April 2010 by Prof. George Gehrels.

Gromet, 2004; Rapela et al., 2007). The existence of a Neoproterozoic DZ peak therefore makes it clear that the metasedimentary rocks trapped deep in the roots of the Famatinian arc were sourced from Gondwanan precursors. This conclusion is not new as it is a common feature in all of the early Paleozoic sedimentary sequences from central and northwestern Argentina (e.g., Adams et al., 2008). However, despite the similar DZ signature with Negro Peinado and Achavil Formations and Mesón Group, the metasedimentary rocks in the Sierra de Valle Fértil occupied remarkably different structural levels during the inception of Early Ordovician Famatinian magmatism. The most important difference is that the metasedimentary rocks studied here were deeply buried and metamorphosed under granulite–facies conditions. In contrast, sedimentary successions of Negro Peinado, Achavil Formations and Mesón Group were never buried deeply enough to attain metamorphic temperatures above greenschist–facies conditions.

Since Thomas and Astini (1996) first hypothesized that the Cuyania/Precordillera microplate was rifted from Laurentia during the Early Cambrian and accreted to West Gondwana during the Middle Ordovician, the geodynamic model has received significant evidence (Naipauer et al., 2010, for a recent review). Moreover, particularly in the Cuyania terrane, geochemical signatures from DZ of Cambrian stratigraphic units have been used to define lithotectonic affinities to continental domains (Finney et al., 2005; Rapela et al., 2007; Naipauer et al., 2010). The close proximity of the eastern boundary of Cuyania to the localities studied here (Fig. 7) allows us to provide additional evidence from a Gondwanan perspective. The combined DZ age spectrum for the Sierra de Valle Fértil represented by 520 and 600 Ma zircon grains, contrasts with the DZ spectra for similar age detritus in the Cuyania terrane (Fig. 6). As observed in several studies (Astini and Dávila, 2004; Benedetto, 2004; Ramos, 2004; among others), this sharp difference among DZ patterns indicates that Cuyania and Sierra de Valle Fértil were amalgamated after Cambrian time.

5.2. Geodynamic evolution of the Famatinian arc

Following the most accurate approach tested by Dickinson and Gehrels (2009) unambiguously indicates a maximum Middle Cambrian depositional age for metasedimentary unit in the Valle Fértil section of the Famatinian arc. These estimated depositional ages are useful to track 25 Ma of evolution starting with sedimentary deposition on offshore basins during the Late Cambrian and ending with burial of sedimentary packages beneath the Early Ordovician arc (see Collo et al., 2009; Ducea et al., 2010).

To address the history revealed by DZ results, it is important to discuss briefly the geological context in which the Famatinian arc was constructed. It is widely accepted that the Early Cambrian Pampean orogeny resulted in deformation and metamorphism of Neoproterozoic and Early Cambrian igneous and sedimentary rocks (Rapela et al., 1998); however, it is still controversial what caused this short-lived and intense tectono-thermal perturbation. The timing of tectonic convergence and metamorphism in the Pampean orogen corresponds closely to a well-known plate re-organization along West Gondwana (Cawood, 2005). This re-organization likely forced major changes along the margin, including the prevention of development of normal subduction zones along some segment of the West Gondwana margin (e.g., Schwartz et al., 2008). As these authors asserted, the geodynamic scenario might have been one of oblique ridge-trench collision followed by migration of a triple junction (Fig. 8A). This hypothesis is highly speculative, but it provides the best account for the voluminous crustal melting, high-temperature metamorphism, structural succession and the pause of subduction-related magmatism that

together are observed in the Pampean orogen (Otamendi et al., 2004).

Following the Pampean orogeny, Upper Cambrian turbidite successions were deposited outboard (Fig. 8B). After deposition, these rocks seem to have followed a rapid path from accretion in a trench-arc system to burial in the mid-crust (Fig. 8C). In the Early Ordovician, accretionary complexes were invaded by deep-seated arc plutonism, resulting in sedimentary successions acting as host rocks for early plutonism, later trapped in the deep crust of the arc (Fig. 8D and E).

The addition of relatively young igneous detritus to turbidite-fan successions suggests the existence of offshore basins in close proximity to an arc that either was waning or shut off a few million years before (see Collo et al., 2009; Adams et al., 2010). The overall paleo-geographic structure would have been similar to those of Cenozoic accretionary orogens in Japan and Alaska (Isozaki, 1996; von Huene et al., 1998). In these settings, turbidite deposits accumulate on submarine slopes and in front of subduction-related arcs during transient-stage magmatic pauses. As most clearly shown by Astini et al. (2007), the uppermost Cambrian angular unconformity separating Negro Peinado and Volcancito formations in the Sierra de Famatina marks the initiation of a new subduction framework (Fig. 8B and C). In fact, this unconformity indicates that by about 490 Ma, deformation of accretionary complexes resulted in crustal thickening and erosion. Formation of the accretionary complex is attributed to an east-dipping subduction zone that disrupted the pre-existing thick Middle to Upper Cambrian turbidite successions (Bahlburg and Hervé, 1997; Astini, 2003). Although part of the same accretionary prism, the sedimentary successions that were underthrust beneath the Famatinian arc would have experienced a different path to be buried beneath the advancing wedge (Fig. 8B; see von Huene et al., 1998; Raimbourg et al., 2009).

For Late Cambrian sedimentary successions to become deeply buried, and then act as the host rocks for Early Ordovician

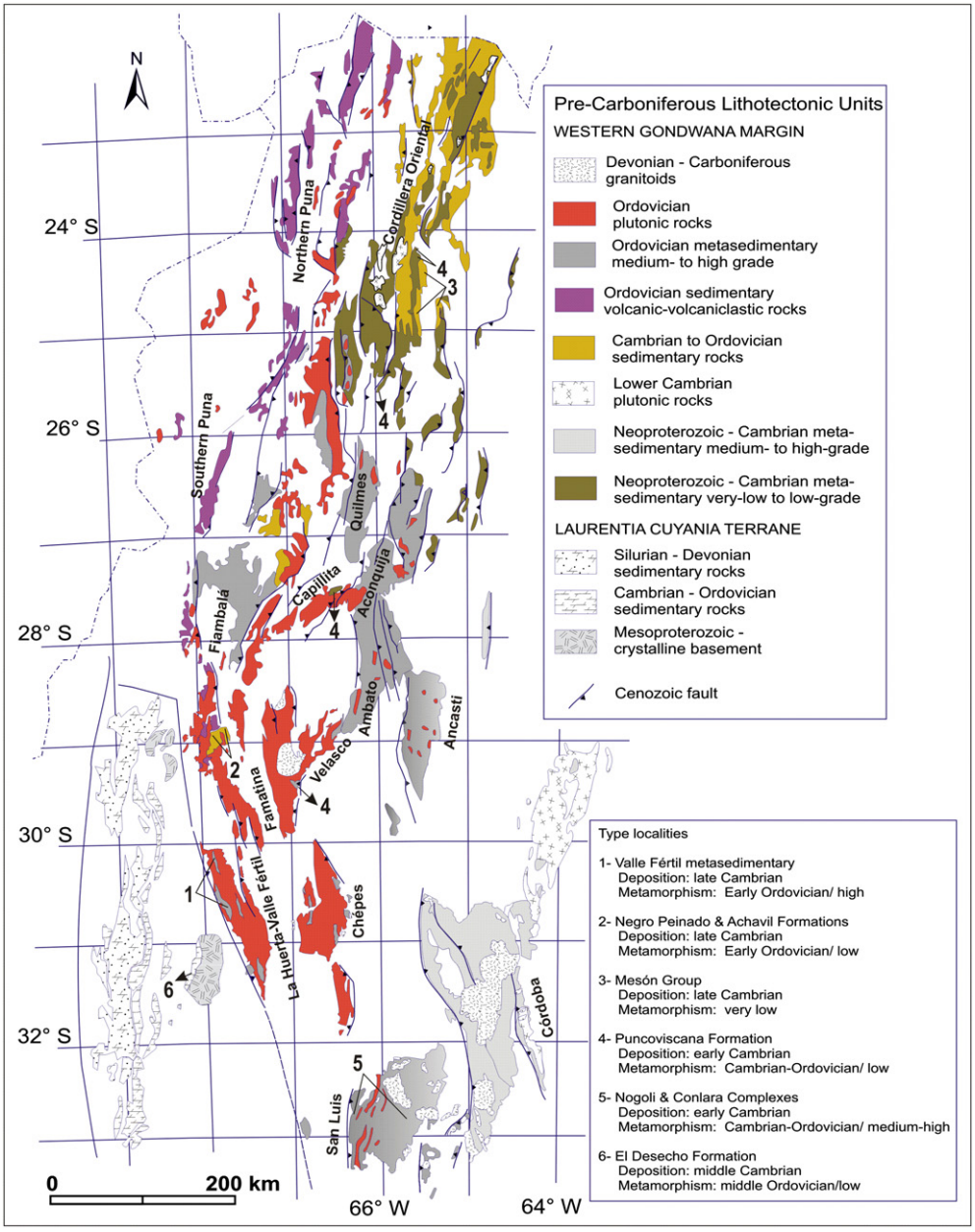

Fig. 7. Distribution of lithostratigraphic units dominated by Neoproterozoic to early Ordovician sedimentary successions over central and northwestern Argentina.

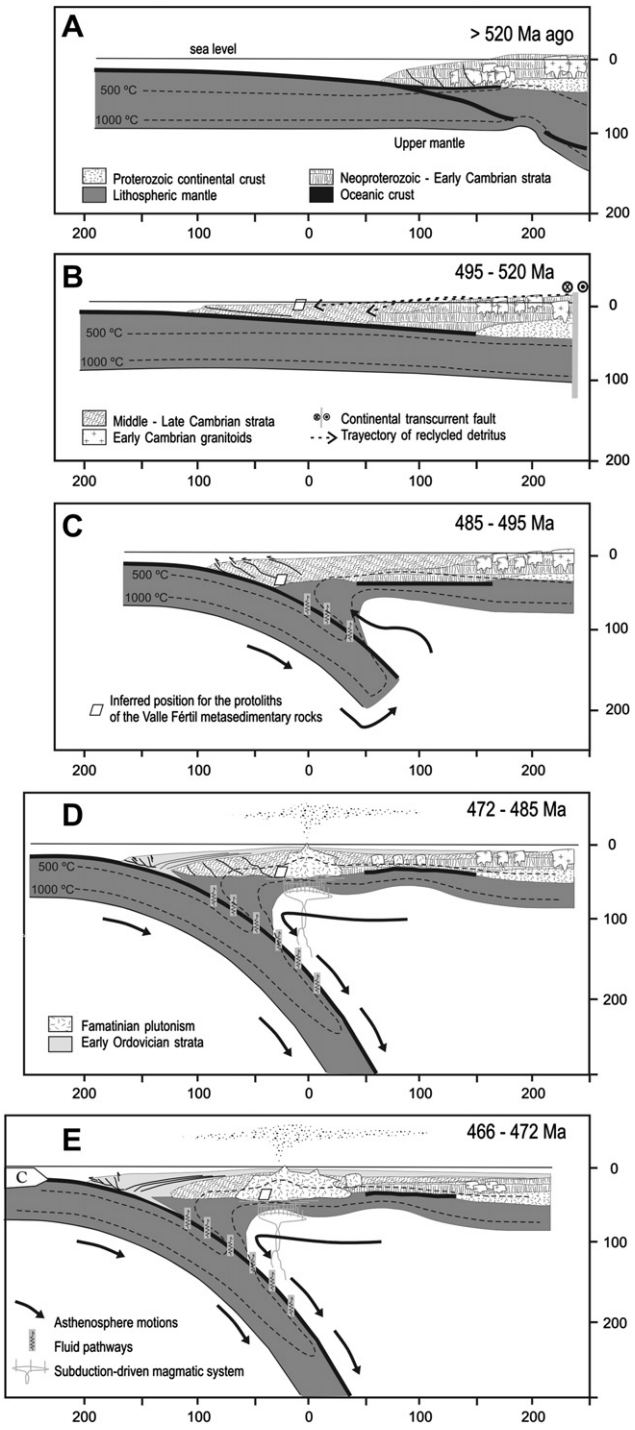

Fig. 8. Schematic crosssection outlining the evolution of the central segment (27–31°S present) of the Famatinian arc during (A) Lower Cambrian; (B) Middle Cambrian, (C) late Upper Cambrian to Lower Ordovician, (D) late Lower Ordovician, and (E) early Middle Ordovician. The Cambrian evolutionary framework is developed after the models by Astini et al. (2007), Rapela et al. (2007) and Schwartz et al. (2008). The calculations by Cloos (1993) were used to construct lithospheric sections that tend to be neutrally buoyant. The simplified thermal model for subduction zones is taken after van Keken et al. (2002). The evolution of infant subduction zones largely reproduces the model by Stern and Bloomer (1992) and Stern (2004). In panel E, the approaching Cuyania "C" microplate is shown (e.g., Benedetto, 2004; Astini and Dávila, 2004).

plutonism, the locus of magmatism must have migrated trenchward (Fig. 8D). During their infancy, most subduction zones seem to experience a stage of rapid oceanward retreat (Stern and Bloomer, 1992; Stern, 2004; Leng and Gurnis, 2011). In such settings, the movement of the slab away from the protoarc causes the main magmatic system to invade early accretionary prisms. Consistent with this view, at least two independent arguments have been put forward supporting the idea that the Famatinian arc was coeval with extension. Using the geochemistry of Famatinian volcanic sequences, Mannheim (1993) showed that the imposition of a bimodal compositional tendency on complete calc-alkaline rock series resembles that of volcanism erupted at rifted arcs. Astini (1998, 2003) also suggested that the opening of intra- and back-arc basins synchronous with subduction-related magmatism requires an extensional regimen. Mafic volcanic rocks from northern Puna to meta-gabbros with MORB signatures from

southern Valle Daza in La Pampa might be taken to record the existence of back-arc magmatism along about 1000 km of the Famatinian arc (Coira et al., 2009; Chernicoff et al., 2010). Another relevant observation is that intra-arc and back-arc basins were filled with a shallow to deep marine sedimentary sequence during the Early and Middle Ordovician (Mángano and Buatois, 1996; Astini, 2003). Rifting and extension would have prevented the closure of intra-arc basins, because the development of a 25-km thick intermediate and silicic Famatinian crust would have led to elevation gain, simply due to isostatic adjustment (e.g., Cloos, 1993).

The final placement of submarine turbidite successions into the deep roots of the Famatinian arc ultimately resulted from plutonic emplacement and associated metamorphism within a pre-existing accretionary complex in an arc setting (Fig. 8D). This process may have happened in many subduction zones throughout Earth's history (Gray and Foster, 1997).

6. Conclusions

The detrital zircon age signature from Sierra de Valle Fértil metasedimentary rocks is dominated by first cycle grains of Lower Cambrian age, and recycled zircon populations derived from Mesoproterozoic (ca. 1000 Ma) and Neoproterozoic (600 Ma) orogenic–magmatic systems. The signature of this detrital zircon pattern is shared by sedimentary strata deposited during Middle and Upper Cambrian times throughout northwestern and central-western Argentina. In contrast, this pattern is distinct from the zircon spectrum of the Neoproterozoic–Early Cambrian Puncoviscana Formation in which the Lower Cambrian age population is minor or absent (Adams et al., 2008, 2010).

The most likely sources of detrital zircon grains in metasedimentary rocks in the deep roots of the Famatininian arc are: 1) sedimentary successions of the Puncoviscana Formation and their low-grade metamorphic equivalents, and 2) igneous and metamorphic rocks crystallized in the Early Cambrian Pampean orogen. Overall, these rocks reflect rapid uplift and erosion of Early Cambrian sedimentary, magmatic and metamorphic rocks into Middle and Upper Cambrian basins that were forming along the paleo-Pacific margin of West Gondwana.

Maximum depositional ages obtained from DZ patterns, in the context of the late Middle Cambrian and Early Ordovician history of the southern West Gondwana margin, lead us to a significant finding: submarine strata deposited during Middle and early Upper Cambrian times may have been buried in accretionary complexes between the uppermost Cambrian and the earliest Ordovician. Subsequently, the accretionary complex was invaded by arc magmatism; to be easily understood, this evolution requires slab retreat. As an end result of less than 40 Ma of geological history, rapidly recycled sedimentary rocks were used to build the arc crust.

Acknowledgements

Thanks to Professors C.J. Chernicoff and M. Naipauer who provided extremely helpful reviews to this manuscript. This work was funded by ANPCYT-Argentina grant PICT 01904/07, by CONICET grant PIP0072 and PICT1299/08, and by a complementary grant from SeCyT-UNRC. Analytical facilities in the Department of Geosciences at the University of Arizona were funded through NSF project NSF-EAR 0910941 from the Tectonics program and ExxonMobil grants.

References

Aceñolaza, F.G., Durand, F.R., 1986. Upper Precambrian-Lower Cambrian biota from the Northeast of Argentina. Geological Magazine 123, 367–375.

Aceñolaza, F.G., Miller, H., 1982. Early Paleozoic orogeny in southern South America. Precambrian Research 17, 133–146.

Adams, C.J., Miller, H., Toselli, A.J., Griffin, W.L., 2008. The Puncoviscana Formation of northwest Argentina: U-Pb geochronology of detrital zircons and Rb-Sr metamorphic ages and their bearing on its stratigraphic age, sediment provenance and tectonic setting. Nenes Jahrbuch für Geologie und Paläontologie-Abhandlungen 247, 341–352.

Adams, C.J., Miller, H., Aceñolaza, F.G., Toselli, A.J., Griffin, W.L., 2010. The Pacific Gondwana margin in the late Neoproterozoic-early Paleozoic: detrital zircon U-Pb ages from metasediments in northwest Argentina reveal their maximum age, provenance and tectonic setting. Gondwana Research 19, 71–83.

Astini, R.A., Dávila, F.M., 2004. Ordovician back arc foreland and Ocloyic thrust belt development on the western Gondwana margin as a response to Precodillera terrane accretion. Tectonics 23, TC4008. doi:10.1029/2003TC001620.

Astini, R.A., Collo, G., Martina, F., 2007. Ordovician K-bentonites in the upper-plate active margin of Western Gondwana, (Famatina Ranges): stratigraphic and palaeogeographic significance. Gondwana Research 11, 311–325.

Astini, R.A., 1998. El Ordovícico en la región central del Famatina (provincia de La Rioja, Argentina): aspectos estratigráficos, geológicos y geotectónicos. Revista de la Asociación Geológica Argentina 53, 445–460.

Astini, R.A., 2003. The Ordovician proto-Andean basins. In: Benedetto, J.L. (Ed.), Ordovician Fossils of Argentina. Universidad Nacional de Córdoba, pp. 1–74.

Bahlburg, H., Hervé, F., 1997. Geodynamic evolution and tectonostratigraphic terranes of northwestern Argentina and northern Chile. Geological Society of America Bulletin 109, 869–884.

Bahlburg, H., Carlotto, V., Cárdenas, J., 2006. Evidence of Early to Middle Ordovician arc volcanism in the Cordillera Oriental and Altiplano of southern Peru, Ollantaytambo Formation and Umachiri beds. Journal of South American Earth Sciences 22, 52–65.

Bahlburg, H., Vervoort, J.D., Du Frane, A., Bock, B., Augustsson, C., Reimann, C., 2009. Timing of crust formation and recycling in accretionary orogens: insights learned from the western margin of South America. Earth-Science Reviews 97, 215–241.

Bahlburg, H., 1998. The geochemistry and provenance of Ordovician turbidites in the Argentine Puna. In: Pankhurst, R.J., Rapela, C.W. (Eds.), The Proto-Andean Margin of Gondwana. Geological Society of London Special Publication, vol. 142, pp. 127–142.

Benedetto, J.L., 2004. The allochthony of the Argentine Prcodillera ten years later (1993–2003): a new paleobiogeographic test of the microcontinental model. Gondwana Research 7, 1027–1039.

de Brito Neves, B.B., Cordani, U.G., 1991. Tectonic evolution of South America during the Late Proterozoic. Precambrian Research 53, 23–40.

Büttner, S.H., Glodny, J., Lucassen, F., Wemmer, K., Erdmann, S., Handler, R., Franz, G., 2005. Ordovician metamorphism and plutonism in the Sierra de Quilmes metamorphic complex: Implications for the tectonic setting of the northern Sierras Pampeanas (NW Argentina). Lithos 83, 143–181.

Castro de Machuca, B., Arancibia, G., Morata, D., Belmar, M., Previley, L., Pontoriero, S., 2008. P-T-t evolution of an Early Silurian medium-grade shear zone on the west side of the Famatinian magmatic arc, Argentina: implications for the assembly of the Western Gondwana margin. Gondwana Research 13, 216–226.

Cawood, P.A., Buchan, C., 2007. Linking accretionary orogenesis with supercontinent assembly. Earth-Science Reviews 82, 217–256.

Cawood, P.A., 2005. Terra Australis Orogen: Rodinia breakup and development of the Pacific and Iapetus margins of Gondwana during the Neoproterozoic and Paleozoic. Earth-Science Reviews 69, 249–279.

Chernicoff, C.J., Zappettini, E.O., Santos, J.O.S., Allchurch, S., McNaughton, N.J., 2010. The southern segment of the Famatinian magmatic arc, La Pampa province, Argentina. Gondwana Research 17, 662–675.

Chernicoff, C.J., Zappettini, E.O., Santos, J.O.S., Godeas, M.C., Belousova, E., McNaughton, N.J., 2012. Identification, zircon U-Pb SHRIMP dating and Hf isotope composition of Lower Cambrian magmatism (El Carancho Igneous Complex) at the boundary between Pampia terrane and the Río de la Plata craton, La Pampa province, Argentina. Gondwana Research 21, 378–393.

Chew, D.M., Schaltegger, U., Kosler, J., Whitehouse, M.J., Gutjahr, M., Spikings, R.A., Miskovic, A., 2007. U–Pb geochronologic evidence for the evolution of the Gondwanan margin of the north–central Andes. Geological Society of America Bulletin 119, 697–711.

Cloos, M., 1993. Lithospheric buoyancy and collisional orogenesis: subduction of ocean plateaus, continental margins, island arcs, spreading ridges, and seamounts. Geological Society of America Bulletin 105, 715–737.

Coira, B., Kay, S.M., Pérez, B., Woll, B., Hanning, M., Flores, P., 1999. Magmatic sources and tectonic setting of Gondwana margin Ordovician magmas, northern Puna of Argentina and Chile. In: Ramos, V., Keppie, J. (Eds.), Laurentia-Gondwana Connections Before Pangea. Geological Society of America Special Paper, vol. 336, pp. 145–170.

Coira, B., Koukharsky, M., Ribeiro Guevara, S., Cisterna, C.E., 2009. Puna (Argentina) and northern Chile Ordovician Basic magmatism: a contribution to the tectonic setting. Journal of South American Earth Sciences 27, 24–35.

Collo, G., Astini, R., Cawood, P.A., Buchan, C., Pimentel, M., 2009. U–Pb detrital zircon ages and Sm–Nd isotopic features in low-grade metasedimentary rocks of the Famatina belt: implications for late Neoproterozoic–early Palaeozoic evolution of the proto-Andean margin of Gondwana. Journal of the Geological Society of London 166, 303–319.

Comínguez, A.H., Ramos, V.A., 1991. La estructura profunda entre Precordillera y sierras Pampeanas de la Argentina: Evidencias de la sísmica de reflexión profunda. Revista Geológica de Chile 18, 3–14.

Cordani, U.G., Sato, K., Teixeira, W., Tassinari, C.G., Basei, M.A.S., 2000. Crustal evolution of the South American platform. In: Cordani, U.G., Milani, E.J., Thomaz-Filho, A., Campos, D.A. (Eds.), Tectonic Evolution of South America: Rio de Janeiro, 31st International Geological Congress, pp. 19–40.

Cordani, U.G., Teixeira, W., D'Agrella-Filho, M.S., Trindade, R.I., 2009. The position of the Amazonia Craton in supercontinents. Gondwana Research 15, 396–407.

Dickinson, W.R., Gehrels, G.E., 2009. Use of U-Pb ages of detrital zircons to infer maximum depositional ages of strata: a test against a Colorado Plateau Mesozoic database. Earth and Planetary Science Letters 288, 115–125.

Drobe, M., López de Luchi, M., Steenken, A., Frei, R., Naumann, R., Siegesmund, S., Klaus Wemmer, K., 2009. Provenance of the late Proterozoic to early Cambrian metaclastic sediments of the Sierra de San Luis (eastern Sierras Pampeanas) and Cordillera Oriental, Argentina. Journal of South American Earth Sciences 28, 239–262.

Ducea, M.N., Otamendi, J.E., Bergantz, G., Stair, K., Valencia, V., Gehrels, G., 2010. Timing constraints on building an intermediate plutonic arc crustal section: U-Pb zircon geochronology of the Sierra Valle Fértil, Famatinian Arc, Argentina. Tectonics 29, TC4002. doi:10.1029/2009TC002615.

Durand, F.R., 1996. La Transición Precámbrico-Cámbrico en el sur de sudamerica. In: Baldis, B.A., Aceñolaza, F.G. (Eds.), Early Paleozoic Evolution in NW Gondwana. Serie de Correlación Geológica, vol. 12, pp. 195–205.

Finney, S., Peralta, S., Gehrels, G., Marsaglia, K., 2005. The Early Paleozoic history of the Cuyania (greater Precordillera) terrane of western Argentina: evidence from geochronology of detrital zircons from Middle Cambrian sandstones. Geológica Acta 3, 339–354.

Gallien, F., Mogessie, A., Bjerg, E., Delpino, S., Castro de Machuca, B., Thöni, M., Klötzlid, U., 2010. Timing and rate of granulite facies metamorphism and cooling from multi-mineral chronology on migmatitic gneisses, Sierras de La Huerta and Valle Fértil, NW Argentina. Lithos 114, 229–252.

Gaucher, C., Frei, R., Chemale Jr., F., Frei, D., Bossi, J., Martínez, G., Chiglino, L., Cernuschi, F., 2010. Mesoproterozoic evolution of the Río de la Plata Craton in Uruguay: at the heart of Rodinia? International Journal of Earth Sciences 100, 273–288.

Gehrels, G.E., Dickinson, W.R., Riley, B.C.D., Finney, S.C., Smith, M.T., 2000. Detrital zircon geochronology of the Roberts Mountains allochthon, Nevada. In: Soreghan, J., Gehrels, G.E. (Eds.), Paleozoic and Triassic Paleogeography and Tectonics of Western Nevada and Northern California. Special Papers Geological Society of America, vol. 347, pp. 19–42.

Gehrels, G.E., Valencia, V.A., Ruiz, J., 2008. Enhanced precision, accuracy, efficiency, and spatial resolution of U-Pb ages by laser ablation-multicollector-inductively coupled plasma – mass spectrometry. Geochemistry Geophysics Geosystems 9, Q03017. doi:10.1029/2007GC001805.

Gray, D.R., Foster, D.A., 1997. Orogenic concepts – applications and definitions: Lachlan Fold Belt, Eastern Australia. American Journal of Science 297, 857–891.

Hongn, F.D., Tubía, J.M., Aranguren, A., Vegas, N., Mon, R., Dunning, G.R., 2010. Magmatism coeval with lower Paleozoic shelf basins in NW-Argentina (Tastil batholith): constraints on current stratigraphic and tectonic interpretations. Journal of South American Earth Sciences 29, 289–305.

von Huene, R., Klaeschen, D., Gutscher, M., Fruehn, J., 1998. Mass and fluid flux during accretion at the Alaskan margin. Geological Society of America Bulletin 110, 468–482.

Isozaki, Y., 1996. Anatomy and genesis of a subduction-related orogen: a new view of geotectonic subdivision and evolution of the Japanese Islands. The Island Arc 5, 289–320.

Ježek, P., Willner, A.P., Aceñolaza, F.G., Miller, H., 1985. The Puncoviscana trough – A large basin of Late Precambrian to Early Cambrian age on the Pacific edge of the Brazilian shield. Geologische Rundschau 74, 573–584.

van Keken, P.E., Kiefer, B., Peacock, S.M., 2002. High-resolution models of subduction zones: implications for mineral dehydration reactions and the transport of water to the deep mantle. Geochemical Geophysical Geosystems 3 (10), 1056. doi:10.1029/2001GC000256.

Larrovere, M.A., de los Hoyos, C.R., Toselli, A.J., Rossi, J.N., Basei, M.A., Beldar, M.E., 2011. High T/P evolution and metamorphic ages of the migmatitic basement of Northern Sierras Pampeanas, Argentina: characterization of a mid-crustal segment of the Famatinian belt. Journal of South American Earth Sciences 31, 279–297.

Leng, W., Gurnis, M., 2011. Dynamics of subduction initiation with different evolutionary pathways. Geochemistry Geophysics Geosystems 12, Q12018. doi:10.1029/2011GC003877.

Lucassen, F., Franz, G., 2005. The early Palaeozoic orogen in the Central Andes: a non-collisional orogen comparable to the Cenozoic high plateau? In: Vaughan, A., Leat, P., Pankhurst, R. (Eds.), Terrane Processes at the Margins of Gondwana Geological Society of London Special Publication, vol. 246, pp. 257–373.

Ludwig, K.R., 2003. Isoplot/Ex 3. Berkeley Geochronology Center, pp. 1–70, (Special Publication).

Mángano, E.G., Buatois, L.A., 1996. Shallow marine event sedimentation in a volcanic arc-related setting: the Ordovician Suri Formation, Famatina Range, northwest Argentina. Sedimentary Geology 105, 63–90.

Mannheim, R., Miller, H., 1996. Las rocas volcánicas y subvolcánicas eopaleozoicas del Sistema de Famatina. Münchner Geologische Hefte 19A, 159–186.

Mannheim, R., 1993. Genese der Vulkanite und Subvulkanite des altpaläozoischen Famatina-Systems, NW-Argentinien, und Seine geodynamische Entwicklung. Münchner Geologische Hefte 7, 1–155.

Mirré, J.C., 1976. Hoja Geológica 19e, Valle Fértil, Provincias de San Juan y La Rioja. In: Servicio Geológico Nacional, Boletín, Buenos Aires, vol. 147, pp. 1–70.

Naipauer, M., Vujovich, G.I., Cingolani, C.A., McClelland, W.C., 2010. Detrital zircon analysis from the Neoproterozoic–Cambrian sedimentary cover (Cuyania terrane), Sierra de Pie de Palo, Argentina: evidence of a rift and passive margin system? Journal of South American Earth Sciences 29, 306–326.

Ogg, J.G., Ogg, G., Gradstein, F.M., 2008. Concise Geologic Time Scale. Cambridge 833 University Press, 177 pp.

Otamendi, J.E., Castellarini, P.A., Fagiano, M.R., Demichelis, A.H., Tibaldi, A.M., 2004. Cambrian to Devonian geologic evolution of the Sierra de Comechingones, eastern Sierras Pampeanas, Argentina: evidence for the development and exhumation of continental crust on the proto-Pacific margin of Gondwana. Gondwana Research 7, 1143–1155.

Otamendi, J.E., Tibaldi, A.M., Vujovich, G.I., Viñao, G.A., 2008. Metamorphic evolution of migmatites from the deep Famatinian arc crust exposed in Sierras Valle Fértil – La Huerta, San Juan, Argentina. Journal of South American Earth Sciences 25, 313–335.

Otamendi, J.E., Vujovich, G.I., de la Rosa, J.D., Tibaldi, A.M., Castro, A., Martino, R.D., 2009. Geology and petrology of a deep crustal zone from the Famatinian paleoarc, Sierras Valle Fértil-La Huerta, San Juan, Argentina. Journal of South American Earth Sciences 27, 258–279.

Pankhurst, R.J., Rapela, C.W., Saavedra, J., Baldo, E., Dahlquist, J., Pascua, I., Fanning, C.M., 1998. The Famatinian magmatic arc in the central Sierras Pampeanas: an Early to Mid-Ordovician continental arc on the Gondwana margin. In: Pankhurst, R.J., Rapela, C.W. (Eds.), The Proto-Andean Margin of Gondwana. Geological Society London Special Publication, vol. 142, pp. 343–368.

Pankhurst, R.J., Rapela, C.W., Fanning, C.M., 2000. Age and origin of coeval TTG, I- and S-type granites in the Famatinian belt of NW Argentina. Transactions of the Royal Society of Edinburgh: Earth Sciences 91, 151–168.

Piñán-Llamas, A., Simpson, C., 2006. Deformation of Gondwana margin turbidites during the Pampean orogeny, north-central Argentina. Geologial Society of America Bulletin 118, 1270–1279.

Raimbourg, H., Tadahiro, S., Asuka, Y., Haruka, Y., Kimura, G., 2009. Horizontal shortening versus vertical loading in accretionary prisms. Geochemistry Geophysics Geosystems 10, Q04007. doi:10.1029/2008GC002279.

Ramos, V.A., Vujovich, G.I., Martino, R.D., Otamendi, J.E., 2010. Pampia: a large cratonic block missing in the Rodinia supercontinent. Journal of Geodynamics 50, 243–255.

Ramos, V.A., 2004. Cuyania, an exotic block to Gondwana: review of a historical success and the present problems. Gondwana Research 7, 1009–1026.

Rapela, C.W., Pankhurst, R.J., Casquet, C., Baldo, E.G., Saavedra, J., Galindo, C., Fanning, C.M., 1998. The Pampean Orogeny of the southern proto-Andes: Cambrian continental collision in the Sierras de Córdoba. In: Pankhurst, R.J., Rapela, C.W. (Eds.), The Proto-Andean Margin of Gondwana. Geological Society of London Special Publications, vol. 142, pp. 181–207.

Rapela, C.W., Pankhurst, R.J., Casquet, C., Fanning, C.M., Baldo, E.G., González-Casado, J.M., Galindo, C., Dahlquist, J., 2007. The Río de la Plata craton and the assembly of SW Gondwana. Earth-Science Reviews 83, 49–82.

Schwartz, J.J., Gromet, L.P., 2004. Provenance of a late Proterozoic–early Cambrian basin, Sierras de Córdoba, Argentina. Precambrian Research 129, 1–21.

Schwartz, J.J., Gromet, L.P., Miró, R., 2008. Timing and duration of calc-alkaline ac of the Pampean orogeny: implications for the Late Neoproterozoic to Cambrian evolution of Western Gondwana. Journal of Geology 11, 29–61.

Stern, R.J., Bloomer, S.H., 1992. Subduction zone infancy: examples from the Eocene Izu-Bonin-Mariana and Jurassic California arcs. Geological Society of America Bulletin 104, 1621–1636.

Stern, R.J., 2004. Subduction initiation: spontaneous and induced. Earth and Planetary Science Letters 226, 275–292.

Thomas, W.A., Astini, R.A., 1996. The Argentine Precordillera: a traveler from the Ouachita embayment of North American Laurentia. Science 273, 752–757.

Tibaldi, A.M., Álvarez Valero, A., Otamendi, J.E., Cristofolini, E.A., 2011. Formation of paired pelitic and gabbroic migmatites: an empirical investigation of the consistency of geothermometers, geobarometers, and pseudosections. Lithos 122, 57–75.

Trompette, R., 1997. Neoproterozoic (~600 Ma) aggregation of Western Gondwana: a tentative scenario. Precambrian Research 82, 101–112.

Turner, J.C.M., 1960. Estratigrafía de la Sierra de Santa Victoria y adyacencias. In: 889 Boletín Academia Nacional de Ciencias de Córdoba, vol. 41, pp. 163–196.

Varela, R., Basei, M.S.A., González, P.D., Sato, A.M., Naipauer, M., Campos Neto, M., Cingolani, C.A., Meira, V.T., 2011. Accretion of Grenvillian terranes to the southwestern border of the Río de la Plata craton, western Argentina. International Journal of Earth Sciences 100, 243–272.

Vaughan, A.P.M., Pankhurst, R.J., 2008. Tectonic overview of the West Gondwana margin. Gondwana Research 13, 150–162.

Vaughan, A.P.M., Leat, P.T., Pankhurst, R.J., 2005. Terrane processes at the margins of Gondwana: introduction. In: Vaughan, A.P.M., Leat, P.T., Pankhurst, R.J. (Eds.), Terrane processes at the margins of Gondwana. Geological Society of London Special Publication, vol. 246, pp. 1–22.

Verdecchia, C.O., Casquet, C., Baldo, E.G., Pankhurst, R.J., Rapela, C.W., Fanning, M., Galindo, C., 2011. Mid- to Late Cambrian docking of the Río de la Plata craton to southwestern Gondwana: age constraints from U–Pb SHRIMP detrital zircon ages from Sierras de Ambato and Velasco (Sierras Pampeanas, Argentina). Journal of the Geological Society of London 168, 1061–1071.

Vujovich, G.I., Godeas, M., Marín, G., Pezzutti, N., 1996. El complejo magmático de la Sierra de La Huerta, provincia de San Juan. In: XIII Congreso Geológico Argentino y III Congreso de Exploración de Hidrocarburos, Buenos Aires, Actas III, pp. 465–475.